smart cities

MDPI

Article

Surface Roughness from Large-Scale Laser Scanning Point Clouds for Urban Accessibility Analysis

Daria Hollenstein, Manuela Ammann, David Eugen Grimm and Susanne Bleisch *

Institute of Geomatics, FHNW University of Applied Science and Arts Northwestern Switzerland, 4132 Muttenz, Switzerland; daria.hollenstein@fhnw.ch (D.H.); manuela.ammann@bluewin.ch (M.A.); david.grimm@fhnw.ch (D.E.G.)

* Correspondence: susanne.bleisch@fhnw.ch

Highlights

What are the main findings?

- We propose a set of surface macrotexture parameters to characterise urban pavement roughness with respect to accessibility.
- Composite descriptors of multiple purpose-designed surface roughness parameters are explored to automatically group and compare surfaces for barrier-free routing.

What are the implications of the main findings?

- Our method is tailored to work with point clouds from TLS, and our results demonstrate the feasibility of the approach when points are within a restricted area around the scanning stations.
- Integrated in routing applications, the method could assist individuals with mobility impairments in travel planning and inform accessible urban planning.

Abstract

Surface macrotexture is of major interest for barrier-free routing, particularly for wheelchair travellers, because it relates to the functional properties of pavements, such as loss of energy through tyre-rolling resistance or vibrational discomfort. These functional properties are difficult to assess. The measurement and characterization of pavement macrotexture, therefore, is a promising approach to support safe route choice for wheelchair travellers and to provide comparative quality criteria for inclusive urban infrastructure management and planning. We use 3D point clouds from terrestrial laser scanning (TLS) and suggest a set of surface roughness parameters tailored to assess the accessibility of urban pavements at the micro-level. We explore the sensitivity of the parameters to point cloud resampling and apply them to a real-world dataset with eleven different pavements. In spite of value variation related to scanning *distance* and *coverage*, our results indicate that combining median-based versions of *Average Roughness* and *Simulated Texture Depth* together with parameters tailored to quantify the depth and proportion of joints and the roughness of the contact area facilitates the grouping and comparison of surfaces regarding barrier-free mobility. The results of this work will be integrated into a framework for accessibility analysis and barrier-free routing.

Keywords: accessibility; digital cities; pavement macrotexture; surface roughness; terrestrial laser scanning; 3D point clouds

Academic Editors: Maria Luisa Tumminello, Elżbieta Macioszek, Anna Granà and Tullio Giuffrè

Received: 6 May 2026
Revised: 27 August 2026
Accepted: 1 September 2026
Published: 7 September 2026

1. Introduction

Walkable cities provide significant ecological, health and economic benefits [1]. Walkable cities require safe pedestrian path networks to provide walkable access to various destinations such as shops, medical services, recreation facilities, or public transport stops [2]. People with motor disabilities may rely on paths without steep slopes or stairs, lowered curbs, and smooth pavements to prevent the risk of falling, the loss of energy through tyre-rolling resistance, or vibrational discomfort [3–5]. Guidelines, e.g., refs. [6,7] and studies, e.g., refs. [3–5,8–10] advocate the use of firm, even pavements with no or narrow joints in the design and construction of accessible public spaces. However, to inform affordance-based barrier-free routing, the multitude of existing surfaces, which vary in smoothness not only by design but also due to wear, need to be assessed at the level of fine-granular geometric properties.

Crowdsourcing information on accessibility [11,12] has potential for barrier-free routing, but the growing availability of area-wide 3D point clouds from photogrammetry and laser scanning should allow for a systematic extraction of micro-level geometric path characteristics. Still, sourcing this information from unstructured data and evaluating routes considering individual needs remains challenging. Functional properties of pavements such as loss of energy through tyre-rolling resistance or ride quality (i.e., vertical accelerations causing vibrational discomfort) are not easily measured over large areas in situ [13,14]. Rolling resistance coefficients are only determined for pavements on level terrain and individual pavement-tyre pairings [15,16]. Induced vibrational discomfort depends on the type and model of walking aid as well as individual disability [17–19]. Therefore, the approximation of functional properties via pavement surface macrotexture characterization is of great interest [14,20] and there is extensive research on the relationship between macrotexture and functional properties of pavements. However, reliably analysing macrotexture, which is in the range of wavelengths between 0.5 and 50 mm (Permanent International Association of Road Congress PIARC), based on 3D point clouds which were recorded with off-the-shelf stationary TLS technologies poses several challenges and is not yet widely established [21]. Typically, data for surface roughness characterization is collected either under laboratory conditions from samples of limited size (around 100 mm $\times$ 100 mm) [22,23] or based on in situ measurements of 2D profiles or 3D swaths with a limited lateral coverage [24,25]. In either case, the data are of very high resolution (<1 mm) and accuracy. Point clouds from stationary TLS technologies, which allow for rapid 3D recording of large outdoor areas, come with a range noise and 3D point accuracy that are far below those techniques (e.g., Leica Geosystems RTC360: range noise 0.4 mm at 10 m, 3D point accuracy 1.9 mm at 10 m [26]). Furthermore, the point density and laser beam-surface intersection angle decrease with increasing distance from the scanning setup. This creates point clouds with inhomogeneous quality and coverage. Combining point clouds from different laser scanning setups mends some of these problems but also creates additional irregularities due to residuals in pairwise registration. To characterise pavement surface roughness reliably and consistently from stationary TLS point clouds, these factors need to be considered and coped with.

The primary contributions of our work are:

- The transfer of concepts of parameter-based pavement macrotexture characterization from material quality analysis to urban accessibility analysis. This includes:
- The development of parameter computation tailored to the analysis of diverse pavements in large-scale, high-density point clouds captured with stationary TLS.
- The design of roughness parameters tailored to characterise key features of pavement accessibility, such as the depth and density of joints and the roughness of the contact area.

https://doi.org/10.3390/smartcities9090146

- The exploration of roughness parameter behaviour with respect to point cloud regions of varying resolution and geometric quality in relation to coverage, distance from the laser scanning setups, and point cloud resampling.

Using roughness parameters to characterise surface smoothness offers the advantage of accommodating previously unknown types of pavement and various stages of wear because the approach does not rely on a classification of surfaces according to known types.

The goal of our work is the identification of surface roughness parameters to characterise and compare pavements with respect to their accessibility. The designed parameters could be used to compare pavements with each other, e.g., known to unknown, and could be combined and weighted for individualised barrier-free routing. The results of this work are currently integrated in a framework for accessibility analysis and barrier-free routing.

2. Related Work

Several studies are focussed on automatic surface classification in the context of barrier-free routing. The proposed approaches can broadly be divided into vibration-based pavement classification and inference on pavement material using imagery or point clouds and machine learning algorithms. In several studies, road surface types are classified using smartphone-based vibration measurements that are collected by wheelchair users [27–30] or vertical acceleration recorded by sidewalk robots [31]. Gani et al. [27] train a machine learning model with 22 features calculated on smartphone gyroscope and accelerometer data to classify standard surfaces into five classes of accessibility. The variance in the signals from different wheelchair models is a challenge when data are crowd-sourced [17]. Recently, this challenge has been addressed with a transfer learning approach [17]. However, acceleration signals are affected by the specific damping effects of the vehicle used as the measuring platform. And the damping effects also propagate to the inference on surface geometry [18]. There is also evidence that the location of measurement on the vehicle influences the resulting signals [19]. Pavement material is also inferred from street view image data with the use of a residual neural network [32] that is trained on a large collection of labelled images [11] which are incorporated with lidar depth information to automatically assess sidewalk accessibility issues, such as cracks, or upended concrete, etc. Hosseini et al. [33] apply an active learning-based framework to segment eight different sidewalk surface classes in street-level images. Treccani et al. [34] use point clouds from laser scanning together with geometric descriptors and a deep learning approach to segment four and five different pavement types, respectively. The application of this approach to a larger variety of pavements is yet pending.

While the application context and overall goal of our work are similar to that of the cited work, we pursue a fundamentally different approach. We draw from the literature on material quality evaluation [23,35] and vehicle-road-interaction research [13,15,22] to identify promising surface roughness parameters and evaluate their stability in large-scale, outdoor application scenarios using point clouds from stationary TLS. The aim is to identify a combination of geometric parameters based upon which relevant surface characteristics are directly inferred without the need for a classification according to known pavement types. This offers the advantage of accommodating previously unknown types and various stages of wear and has the potential to lead to fine-grained roughness rankings within and across different surface types. Approaches to leverage a relation between surface geometry and functional properties, i.e., acoustic diffusion, have also previously been tried in the general semantic understanding and segmentation of point clouds [36].

State-of-the-art research in material quality evaluation involves the computation of a set of descriptive and discriminative surface roughness indices from digital 3D data, e.g., [20,21,23]. Frequently used roughness indices in studies on rolling resistance or ride quality include *Mean Profile Depth* (MPD) [37] and *Mean Texture Depth* (MTD) [38]. With the advance of 3D capturing technologies, attempts were made to automate their computation from digital 3D data. *Simulated Mean Texture Depth* (SMTD) [22] was proposed as a simple digital alternative to MTD. On the other hand, measures calculated on the material distribution of a pavement profile or a surface are used to characterise macrotexture, particularly in relation to skid resistance (e.g., [39]). Measures on the material distribution are used to characterise a pavement with respect to different vertical sections of its profile or surface, i.e., the peak area, the core area, and the valley area. Senthilvelan et al. [20] calculate, amongst others, *Valley Material Ratio* and *Area of Peaks* as defined in ISO 25178-2:2021 [40] on sections of 3D data that have a horizontal resolution <0.1 mm in the x- and y-directions. Our proposed parameters, *Joint-Surface Ratio* and *Roughness of the Contact Area* (see Section 3.3), similarly quantify properties at specific vertical sections of the surface; however, the computation considers the peculiarities of the 3D measurements from TLS and is targeted at geometric properties that are directly relevant for the travelling comfort and safety of people with reduced mobility. While traditionally, studies on surface macro- and microtexture address roads and motor vehicles, more recently, sidewalk material quality has also been examined with respect to friction and skid resistance [18,25]. Jiang et al. [25] integrate data from a high-resolution profile laser scanner (0.15 mm in the x- and 0.019 mm in the z-direction, field of view: 1 m) with friction coefficient measurements to examine the relation between skid resistance and sidewalk material. Vertical measurement platform acceleration is also utilised to infer continuous sidewalk smoothness indicators [18,31]. However, vibration-based inference on surface quality suffers from the above-mentioned limitations.

3. Methods

We study the behaviour of different roughness parameters for varying conditions in input data and computation, with the objective of defining quality requirements for point clouds from stationary TLS and assessing the stability of several surface roughness parameters in large-scale application scenarios. In particular, we examine the effects of point cloud resampling and distance to the nearest laser scanning setup on parameter values. These factors likely affect surface roughness estimation [23,41].

Subsequently, we describe the data capturing process, the choice and calculation of surface roughness parameters, and the test data sets used in the analyses.

3.1. Data Collection

For our study we use real-world data, which was acquired using a Leica RTC360 terrestrial laser scanner by Leica Geosystems, part of Hexagon, Heerbrugg, Switzerland. 105 setups were scanned with a resolution of 6 mm at 10 m to cover the test area with the desired resolution of at least 1 point per cm^2 (Figure 1). Four additional setups were scanned outside the test area in Figure 1 to capture pavement D. The specified range noise of the RTC360 is 0.4 mm at 10 m and the specified 3D point accuracy is 1.9 mm at 10 m [26]. Laboratory studies indicate that up to 8 m from the scanning station, the range noise may be below the specified level for various target materials [42]. The individual scans were registered automatically using the Visual Inertial System (VIS) technology of the RTC360. VIS uses a combination of an integrated inertial measurement unit and a camera system to run a Simultaneous Localization and Mapping (SLAM) algorithm [43]. The final registration to combine the individual laser scans was calculated using the cloud-to-cloud registration method in the software Leica Cyclone REGISTER 360 [44] by Leica Geosystems, part of Hexagon, Heerbrugg, Switzerland. The overall registration quality is better than 8 mm with a mean deviation of 4 mm.

https://doi.org/10.3390/smartcities9090146

To be able to combine the current data with the results of future surveys in the same area, the cadastral reference points were used for georeferencing. A Leica MS60 MultiStation was used to measure the reference points and the laser scanning targets (checkerboard patterns), which were well distributed over the area. All targets were measured twice from different stations and had an average deviation of 0.7 mm, 1.4 mm, and 0.7 mm, and a maximum deviation of 6 mm, 7 mm, and 6 mm for the x-, the y-, and the z-axis, respectively. Multiple measurements of targets were averaged and used for georeferencing the scans. Data on pavement D is not georeferenced.

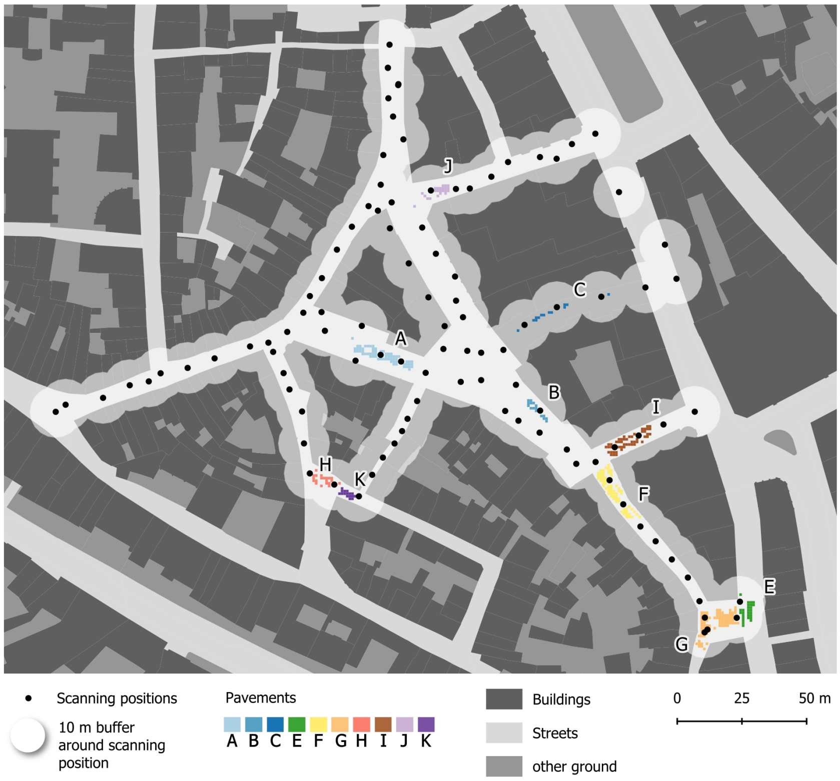

Figure 1. Map of the study area with positions of laser scanning setups, point cloud coverage and location of pavement samples in data set II. The samples are colour-coded according to pavement type A–K. Pavement D is outside the displayed area. (Data of background map: Grundbuch- und Vermessungsamt Kanton Basel-Stadt 2026).

3.2. *Pavement Types and Visual Evaluation of Their Accessibility*

Eleven pavement types, which differ from each other with respect to material, surface treatment and joints, were identified in the study area and manually segmented in the point cloud. The surface types are labelled with capital letters from A to K (Figures 2 and 3). The order of letters tentatively reflects their descending suitability for wheelchair travellers. Decisive factors for the accessibility of pavements are the presence and quality of joints and the smoothness of the surface. A preliminary ranking of the eleven pavements was established based on guidelines on barrier-free route design [6,7,45]: Based on [6,7], the eleven pavements were grouped into three broad classes without further differentiation. SIA 500 [45], on the other hand, differentiates five classes. However, the provided criteria are not detailed enough to support the unambiguous classification of all eleven types. Following the guidelines [6,46] regarding the definitive assessment of the given pavements, the ranking A–K was established based on an on-site expert interview [47] and subsequently discussed and substantiated with two wheelchair users. The ranking A–K is tentative in the sense that surface types J and K are clearly less favourable than A, B and C; however, the pairwise ranking of, e.g., D–F or H–J is less clear. For example, pavements D, E and

F are similar. D is made of smoothed boulders with angular edges, while cobblestones in F are not cut but nearly level with edges gradually merging into joints. Type E displays variable quality due to effects from wear and its ranking with respect to D and F is not clear cut. In fact, different surface types may be equally unsuitable for wheelchair travel due to different geometric properties. Still, A, B and C will be more favourable than D–F, while H–K will be less favourable. In the area with type C, there are data quality issues due to strong laser beam reflectance by the polished tiles. In the area of type A, there may be data quality issues due to difficulties in cleanly separating ground points from other objects. It must be pointed out that only pavements A-C are suited for wheelchair travel.

	Description /	SN 640 075	SIA 500	Photo	Cyclone 3DR surface flatness analysis (0.1m neighbourhood)
A	Asphalt	1	1		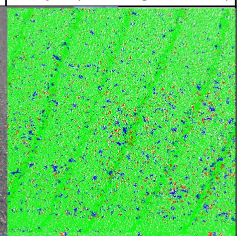
B	Concrete stone, interlocking paving stone	1	1		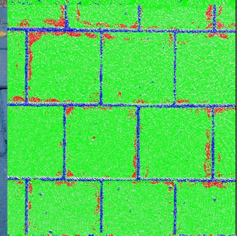
C	Stone tiles, polished	1 / 2	1		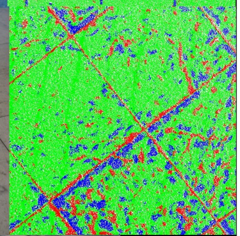
D	Natural stone paving, smoothed, grouted	2	1 – 3		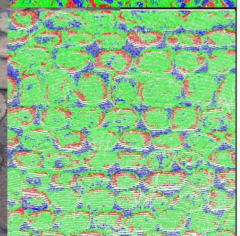
E	Natural stone paving, cut, grouted	2	2 – 3		
F	Bouldering, level, grouted	3	?		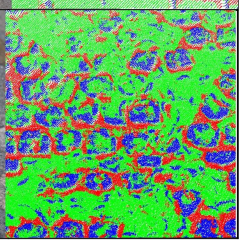

	Description /	SN 640 075	SIA 500	Photo	Cyclone 3DR surface flatness analysis (0.1m neighbourhood)
G	Cobblestone, cut, grouted	3	3		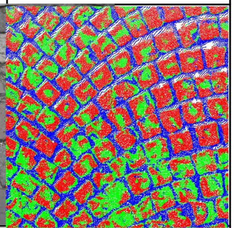
H	Bouldering, grouted	3	4 – 5		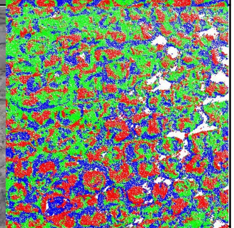
I	Cobblestone, raw, grouted	3	4		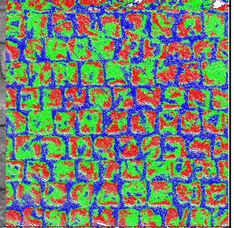
J	Cobblestone, cut	3	5		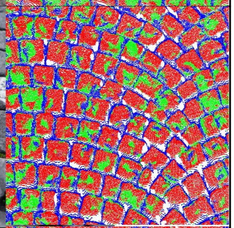
K	Bouldering, strongly vaulted	3	5		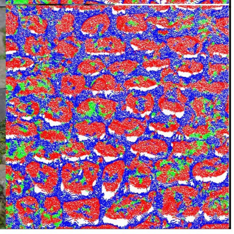

Figure 2. Pavement types identified within the scanned area and ordered tentatively according to their descending suitability for wheelchair users from A to K based on an expert interview. In columns SN 640 075 [7] and SIA 500 [45], the pavements are graded according to the respective guideline (SN 640 075: 1: good, 2: limited suitability, 3: unsuited; SIA 500: 1: good, 2: suitable, 3: limited suitability, 4: little suitability, 5: unsuited). SIA 500 rates pavements with respect to rolling resistance and comfort, risk of tripping, and skid resistance. We did not consider the latter, since skid resistance is related also to pavement microtexture, which is out of the scope of the chosen data acquisition technology.

3.3. Surface Parameters

Surface characteristics that are likely related to accessibility are width, depth, and shape of joints; joint-surface ratio; and the roughness of the contact area [6]. To approximate these properties, we calculate two roughness parameters, which are used to characterise surfaces in the context of road-vehicle interaction [15,22] and material quality evaluation [23,35]: *Average Roughness* and *Simulated Mean Texture Depth* (SMTD). These parameters are usually measured and quantified according to standards and not with the use of 3D point clouds from TLS [23,35]. Hence, we adapt data processing and parameter computation to cope with the inhomogeneous nature of the TLS data. Also, we define three additional parameters to characterise surfaces with respect to joint depth J_m, joint-surface-ratio J_r, and with respect to roughness of the contact area R_o.

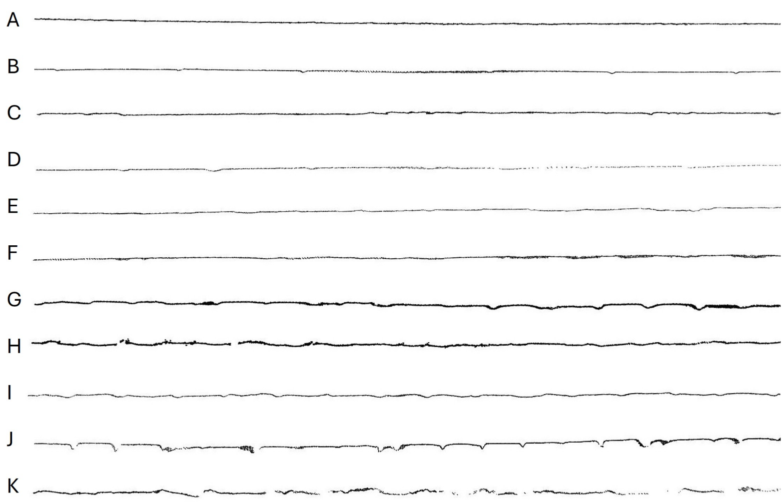

Figure 3. Lateral view on sections of the reference sample for each pavement (A–K). Pavement A was rated most accessible; pavement K was rated least accessible in an expert evaluation.

The general procedure of parameter calculation is as follows (Figure 4): First, the point cloud is optionally resampled in Leica Cyclone 3DR [48] to create data with more evenly spaced points and to reduce the computational load of the following parameter calculation. The resampling algorithm estimates a local surface for each cell of a regular grid with a user-defined spacing and retains the point closest to that surface. For data set I (c.f. Section 3.3.1), we use resampling distances of 2 mm, 5 mm, 10 mm and 20 mm. Data set II (c.f. Section 3.3.2) is resampled to an average point distance of 10 mm. After the resampling, local planes are fitted to the point cloud for each cell of a regular 0.1 m $\times$ 0.1 m grid using a least-squares method. An interval of 0.1 m is commonly used in surface macrotexture analysis, as it yields point-wise deviations from the plane at a spatial frequency that reflects macrotexture (0.5–50 mm) [13], cf. Figure 2. Larger neighbourhoods will return information on surface levelness and obstacles (wavelengths > 50 mm), smaller neighbourhoods, could provide information on microtexture. However, the latter cannot be expected with the present TLS data, because the wavelengths of microtexture (<0.5 mm) are within the range noise of the laser scanner [26]. To control for undesirable effects of point cloud co-registration, data from multiple setups are processed separately up to this step. After the plane fitting, outliers are removed (deviations > 25 mm, c.f. Section 4.3), and parameter values are calculated based on the height deviation values of all points within a sampling unit (e.g., 1 m $\times$ 1 m). Python NumPy 2.1.0 [49] was used for plane fitting and parameter computation.

- *Average Roughness* (R_a) is calculated as the mean absolute deviation from the fitted plane considering the deviation z_i of all points in the sampling unit, as in [35]. In addition, we calculate the median instead of the mean (R_m: *Median Roughness*) to improve parameter robustness with respect to varying distance from the laser scanning setups and outlier influence.

$$R_a = \frac{1}{n} \sum_{n=1}^{n} |z_i| \tag{1}$$

$$R_m = Median(z) \tag{2}$$

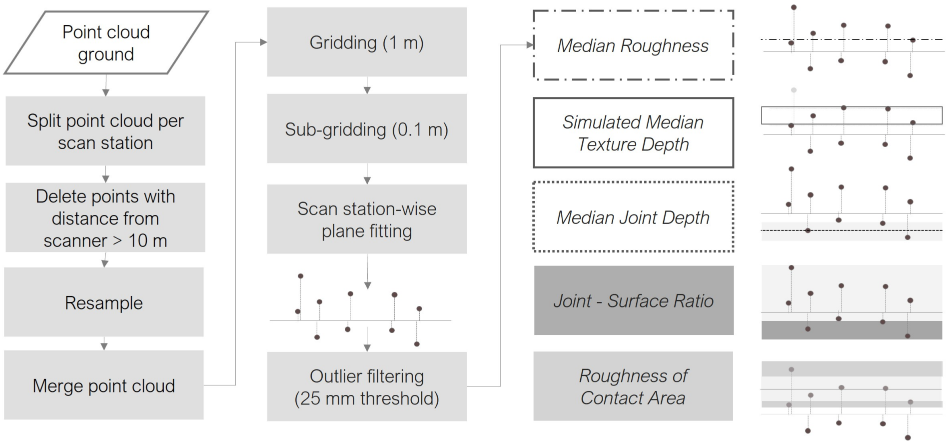

Figure 4. Steps of point cloud processing and parameter computation. The signature of outlines and backgrounds of parameter names in the third column corresponds with that of lines and areas in the diagrams of the rightmost column which illustrate the computation of the respective parameter.

- *Simulated Mean Texture Depth* (SMTD) is calculated similar to [22]. In adaptation to our data, we use the 95th percentile instead of the maximum value in the calculation of SMTD to reduce outlier influence. In addition, we propose a calculation using the median instead of the mean (SMdTD) to improve parameter robustness with respect to varying distance from the laser scanning setups and outlier influence.

$$SMTD = \frac{1}{n}\sum_{n=1}^{n}\{Q_{95} - z_i | z_i < Q_{95}\} \tag{3}$$

$$SMdTD = Median(\{Q_{95} - z_i | z_i < Q_{95}\}) \tag{4}$$

- *Median Joint Depth* (J_m) is calculated as the median of the values deviating more than $d = -1$ mm from the fitted plane. For surfaces, like the pavements in Figure 2, this parameter may reflect joint depth. The threshold of -1 mm was chosen empirically. It is a threshold below which points clearly belong to joints for all pavements in the present data set, as seen from Figure 2. Joint areas would be missed if the threshold were increased, and decreasing the threshold would turn J_m into a more general parameter of surface roughness. To facilitate comparison of J_m with other parameter values, the absolute value of the median is returned, such that a high J_m indicates more pronounced joints.

$$J_m = Median(\{z_i | z_i < d\}) \tag{5}$$

- *Joint-Surface Ratio* (J_r) is the proportion of points more than 1 mm below the fitted plane.

$$J_r = \frac{1}{n}\sum_{n=1}^{n} 1_{\{z_i<d\}} \quad where \;\; 1_{\{z_i<d\}} = \begin{cases} 1 & \text{if } z_i < d \\ 0 & \text{else} \end{cases} \tag{6}$$

- *Roughness of the Contact Area* (R_o): After the plane fitting, the resulting deviations are shifted by subtracting the mean of the most frequent 1 mm-value bin. The bin containing most values after plane fitting is expected to hold the strongest signal of the actual contact surface of the pavement. After the shifting, all points with deviations larger than –1 mm are input to a new plane fitting process. R_o is computed as the proportion of resulting deviations with absolute values ≥ 1 mm. Setting the threshold for this computation to 1 mm follows as a consequence from the threshold for joint depth and joint density analysis.

In the following, the proposed surface roughness parameters are calculated on two distinct data sets derived from the collected laser scanning point cloud (Section 3.1).

3.3.1. Data Set I

Data set I serves as a reference to explore the effects of resampling and sampling unit size. Data set I contains points from only one laser scanning setup per pavement A–K to control for variation that is introduced when pooling points from multiple setups. We also tried to control for strong variations in point densities and angles of intersection between the laser beam and the surface by selecting areas of 2 × 2 m within the vicinity of the scanner setup. The average point distance for each 2 × 2 m sample is listed in Table 1. The point cloud sections were resampled to average point distances of 2 mm, 5 mm, 10 mm and 20 mm. Surface parameter values were computed for two different sampling unit sizes, 1 m × 1 m and 0.5 m × 0.5 m. This results in ten different data sets (2 × 5). We chose 0.5 m as the minimal sampling unit side length, as we expect this size to minimally cover the joint–surface pattern of the pavements included in the study. The units of side length 1 m each contain exactly four of the smaller 0.5 m × 0.5 m-units and approximately correspond to the space minimally required by a wheelchair (c.f. [6]).

Table 1. Average point distance and point distance standard deviation in the non-resampled point cloud at surface type reference locations.

Type	Average Point Distance in mm	Standard Deviation in mm
A	1.3	1.8
B	1.9	2.5
C	1.6	2.3
D	1.7	2.4
E	4.3	6.7
F	1.8	2.3
G	1.6	2.1
H	1.7	2.1
I	1.8	2.3
J	1.7	2.4
K	1.5	2.1

After calculating the parameters according to Section 3.3, the units were filtered based on point density and point distribution in the original, non-resampled point cloud to prevent poorly covered cells from going into the analysis. For all but two pavement types, at least one 1 m × 1 m unit contained four sub-cells of side length 0.5 m, which were well covered with points. For two pavements, only three of the four sub-cells were fully covered.

3.3.2. Data Set II

A second set of data was constructed using all points within 10 m from the laser scanning setups. Data set II is used to explore the stability of parameters and their suitability for characterizing and ranking pavements in real-world TLS data. To ensure approximately equal point densities across the samples, the input data were resampled to an average point distance of 10 mm and grid cells that contained less than 100 points every 0.1 m × 0.1 m were discarded. We also excluded samples with features that interrupt the pattern of the pavement (manhole cover, gutters, etc.) to ensure homogeneity of surface characteristics for the samples of the same pavement type.

4. Results

In Section 4.1, results on parameter value variation related to resampling are presented. In Sections 4.2 and 4.3, the usability of the parameters for the characterization of larger point clouds from multiple laser scans is reported.

4.1. Influence of Resampling on Parameter Variation

The influence of resampling on parameter variation is studied using the single scan reference data set I. Two different sampling unit side lengths, 0.5 and 1.0 m, are compared. Figure 5 shows the values for each surface roughness parameter for every pavement type (A–K) at each level of resampling (no resampling, or resampling to 2 mm, 5 mm, 10 mm, or 20 mm average point distance). In the graph, points indicate results for the 1.0 m × 1.0 m sampling units, and bars span the range of values for the corresponding 0.5 m × 0.5 m cells. In Table 2, we report the coefficient of variance ($CV = \frac{sd}{mean}$) per pavement for the two sampling unit sizes.

Table 2. Coefficient of variance CV for identical sampling units under resampling to 2 mm, 5 mm, 10 mm, 20 mm for units of size 1 m × 1 m (top) and 0.5 m × 0.5 m (bottom) in data set I.

Type	R_a	R_m	$SMTD$	$SMdTD$	J_m	J_r	R_o
A	0.02	0.02	0.03	0.04	0.02	0.07	0.37
B	0.06	0.06	0.06	0.07	0.06	0.09	0.29
C	0.03	0.03	0.04	0.04	0.02	0.06	0.07
D	0.03	0.03	0.03	0.03	0.01	0.02	0.57
E	0	0.01	0.01	0	0.01	0	0.22
F	0.02	0.02	0.02	0.02	0.01	0.03	0.45
G	0	0.01	0.01	0.01	0.01	0.01	0.18
H	0.01	0.01	0.01	0.01	0.01	0.01	0.15
I	0.01	0.01	0.01	0.03	0.01	0.01	0.37
J	0.07	0.08	0.11	0.14	0.05	0.04	0.17
K	0.01	0.02	0.02	0.04	0.01	0.02	0.02
A	0.11	0.15	0.11	0.12	0.02	0.27	0.49
B	0.07	0.08	0.08	0.08	0.07	0.1	0.33
C	0.07	0.09	0.07	0.07	0.03	0.13	0.17
D	0.10	0.1	0.11	0.11	0.05	0.15	0.53
E	0.05	0.06	0.07	0.08	0.05	0.05	0.38
F	0.06	0.06	0.06	0.04	0.04	0.07	0.44
G	0.03	0.02	0.04	0.08	0.05	0.02	0.17
H	0.07	0.07	0.08	0.09	0.04	0.05	0.47
I	0.03	0.03	0.03	0.05	0.02	0.02	0.42
J	0.14	0.12	0.15	0.16	0.12	0.04	0.2
K	0.08	0.08	0.09	0.1	0.1	0.03	0.15

The CVs for parameter values of R_a, R_m, $SMTD$, $SMdTD$, and J_m in the 1.0 × 1.0 m sampling units are ≤5%, for all pavements except B (6–7%), and J (7–14%). Parameter values for pavement B drop pronouncedly, when the point cloud is resampled to an average point distance of 20 mm. Apparently, at that level, the narrow joints of pavement B are partly missed, and the values of parameters diminish. The same occurs for values of J_r. An interpretation for the variance of values for pavement J is more difficult. Further, R_a, R_m, SMTD, SMdTD, J_r, and R_o, are generally higher than expected for pavement C. This is due to the strong reflectance of the polished surface which leads to errors in the point cloud, as seen from Figure 2 and from the wiggles in the profile of pavement C in Figure 3. Overall, R_a, R_m, $SMTD$, and $SMdTD$, and J_m remain stable under resampling of 1 m × 1 m units down to an average point spacing of 10 mm, with exception of pavement J (Figure 2). The ranking of pavements is not affected by the variation related to resampling.

For 0.5 m × 0.5 m sampling units, parameter values vary more strongly: CVs for J_m are within 10% (except J: 12%) and CVs for R_a, R_m, $SMTD$, $SMdTD$ are within 15%. The observed variation of parameter values for 0.5 m × 0.5 m units is not visibly related to the level of resampling (Figure 5). Again, CVs for pavement J are the highest.

For the median-based R_m and $SMdTD$ and the mean-based R_a and $SMTD$, the picture is broadly the same. However, the overall range of values diminishes for R_m and $SMdTD$

compared to $SMTD$ and R_a. This is true for sampling units of both sizes. The variation of values related to resampling is slightly stronger when the median is used instead of the mean. The pavement rankings by R_a and R_m as well as the rankings by $SMTD$ and $SMdTD$ are in close correspondence with each other and mostly in correspondence with the ranking as proposed in Section 3.2. However, the use of the median-based $SMdTD$ slightly improves this correspondence.

J_r is affected more strongly by increased levels of resampling (10 mm, 20 mm) and values for 0.5 m × 0.5 m units scatter pronouncedly (Figure 5). CVs for 1 m × 1 m units are below 5% except for the smoothest pavements: A (7%), B (9%) and C (6%).

R_o is not stable across levels of resampling (Figure 5). CVs for R_o range from 2 to 57% according to pavement type. The scattering is not clearly related to the level of resampling. However, considering the non-resampled point cloud and the minimally resampled point cloud (2 mm average point distance) as the reference, the ranking of the 1.0 × 1.0 m units mostly reflects the targeted property of the pavements, except for type C and potentially type H. For C, the resulting values are higher than expected. This is due to errors in data caused by strong laser beam reflectance. The roughness of the contact surface of H is potentially underestimated by R_o. For pavement F, the results are inconclusive.

To summarise the influence of resampling on data set I: The values of parameters R_a, R_m, SMTD, SMdTD, J_m and J_r are mostly stable; when the point cloud is resampled to 2 mm, 5 mm, or 10 mm, the values of R_o show a large variance. The reduction of the size of the sampling unit increases the variance of parameter values. However, the mean value of the four 0.5 m × 0.5 m units is close to the value of the corresponding 1.0 × 1.0 m unit, except for values of R_o.

4.2. Full Point Cloud Analysis

Figures 6–8 summarise the results of parameter computation on data set II. The figures give an indication, of whether the proposed parameters group similar pavements and separate dissimilar pavements with respect to the targeted property. In addition, Figures 6 and 7 provide evidence for improved stability and discriminative power of parameters R_m and $SMdTD$ compared to R_a and $SMTD$, respectively.

The analysis of the multi-scan data set II indicates a reduction of the type-wise inter-quartile ranges and the spans for the median-based parameters R_m and $SMdTD$ (Figures 6 and 7) compared to the mean-based versions R_a and $SMTD$. At the same time, the span of medians for $SMdTD$ is stable relative to $SMTD$ and is only slightly reduced for R_m relative to R_a. Compared with R_a, the use of R_m strongly reduces the overlap of value ranges for pavements of clearly different roughness (e.g., A–C vs. D–F).

For overall roughness parameters, R_m and $SMdTD$ (Figures 6 and 7), the order of median values for pavements is mostly in correspondence with the expert's evaluation (c.f. Section 3.2) and changes little relative to the order of samples in data set I (c.f. Figure 5). The same is true for J_m and J_r (Figure 8). The jointless pavement, A, is at the lower end of the scale of J_m, followed by C, then D and F, which have large but shallow joints, followed by grouted pavements G and I, and pavement B with narrow but deep joints. The non-grouted pavements J and K are at the top of the scale. The values of J_r for pavements D and F exhibit considerable dispersion. D and F are pavements with large, shallow joints. The value variance is probably due to the masking of some of the joint areas by the 1 mm threshold while other joints may be broad enough to be at the centre of the plane fitting (c.f. Figure 2). Otherwise, groups of similar pavements are matched by J_r. The ranking of pavement median values for R_o is mostly as expected with respect to the targeted property. This is inferred from Figures 2 and 3: Pavements A, B and C are expected to score similarly and at the lower end of the parameter scale. Pavements D, E, G, and F, which all have

https://doi.org/10.3390/smartcities9090146

treated surfaces, should follow. Pavement J should score slightly higher than this group, because even though the cobble stones are flat, the pavement has been in use for a long time, and in many places parts of the cobble stone surfaces are chipped. Stone pavements with raw surfaces, I, H, and K are expected at the upper end of the scale. Applied to the multi-setup data, R_o does not stand out with respect to within-type variability.

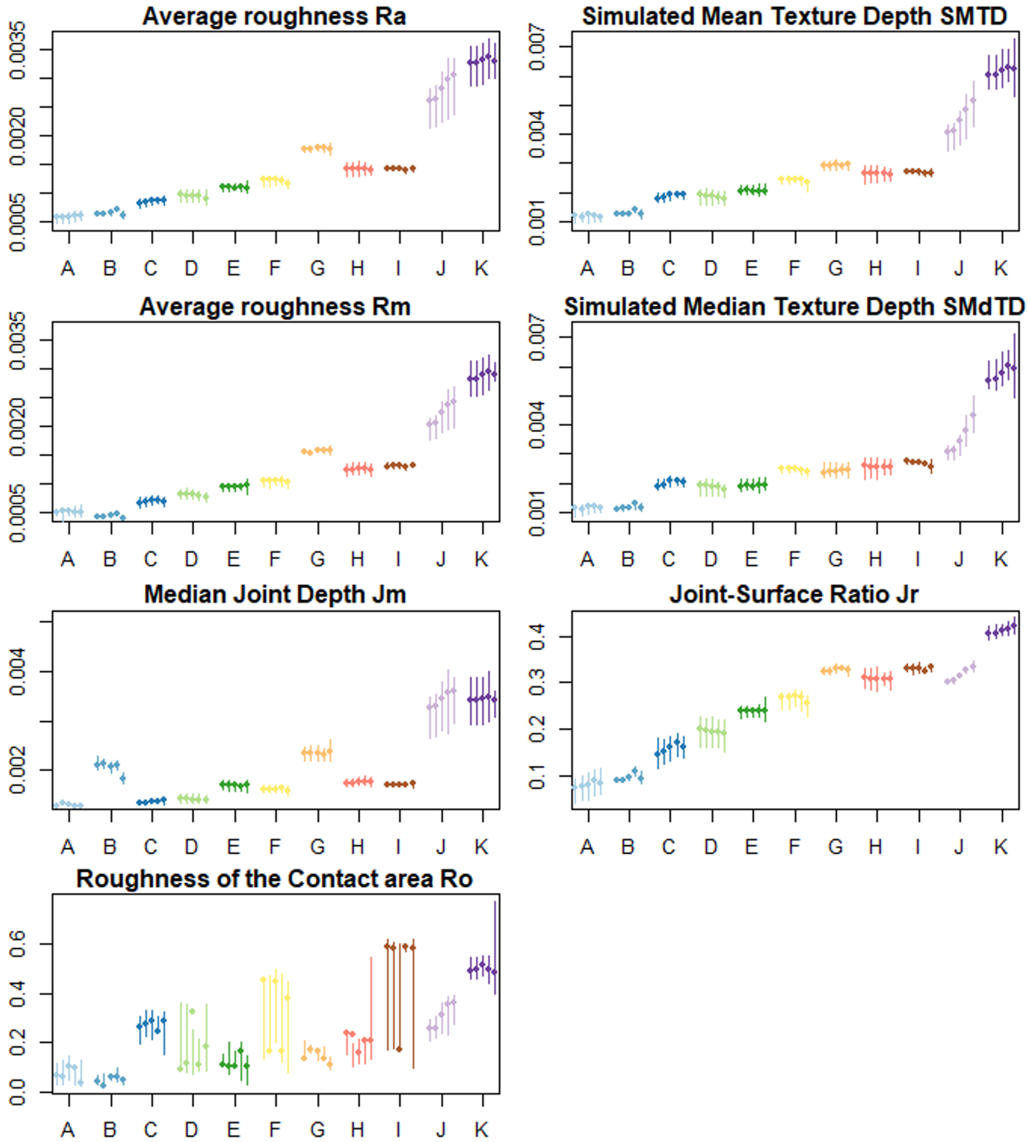

Figure 5. Parameter sensitivity to point cloud resampling: Circles indicate parameter values computed on 1 m × 1 m sampling units; vertical lines indicate the value ranges of the respective 0.5 m × 0.5 m sub-cells along the y-axis for each pavement type (A–K, colour-coded) and each level of resampling (per pavement type, from left to right: not resampled, 2 mm, 5 mm, 10 mm, 20 mm average point distance). The top row shows results for mean-based *Average Roughness* R_a and $SMTD$; the second row shows results for the median-based versions of these parameters, R_m and $SMdTD$. Y-axis units for R_a, R_m, $SMTD$, $SMdTD$ and J_m: m; y-axis for J_r and R_o are unitless (theoretical range: 0–1). We do not expect that the ranking of pavements by J_m and J_r corresponds with the ranking by *average* roughness or *Simulated Texture Depth*. Large but shallow joints do not necessarily lead to high overall roughness.

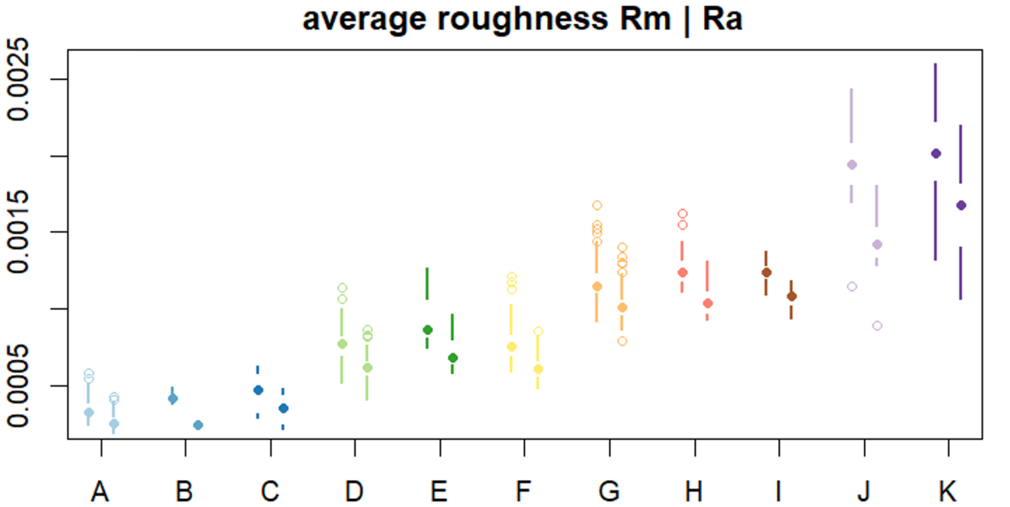

	Min.	1st Qu	Median	3rd Qu	Max.	Interqu. R.	Span
A	2×10^{-4}	2.4×10^{-4}	2.6×10^{-4}	3×10^{-4}	4.3×10^{-4}	6.5×10^{-5}	2.4×10^{-4}
	2.5×10^{-4}	3×10^{-4}	3.3×10^{-4}	3.9×10^{-4}	5.9×10^{-4}	9.3×10^{-5}	3.4×10^{-4}
B	2.2×10^{-4}	2.4×10^{-4}	2.5×10^{-4}	2.6×10^{-4}	2.8×10^{-4}	2.2×10^{-5}	5.4×10^{-5}
	3.8×10^{-4}	4.1×10^{-4}	4.2×10^{-4}	4.6×10^{-4}	4.9×10^{-4}	4.9×10^{-5}	1.1×10^{-4}
C	2.2×10^{-4}	2.5×10^{-4}	3.5×10^{-4}	4.5×10^{-4}	4.9×10^{-4}	1.9×10^{-4}	2.6×10^{-4}
	3×10^{-4}	3.2×10^{-4}	4.8×10^{-4}	5.8×10^{-4}	6.3×10^{-4}	2.6×10^{-4}	3.3×10^{-4}
D	4.2×10^{-4}	5.6×10^{-4}	6.2×10^{-4}	6.6×10^{-4}	8.7×10^{-4}	9.9×10^{-5}	4.5×10^{-4}
	5.2×10^{-4}	6.9×10^{-4}	7.7×10^{-4}	8.4×10^{-4}	1.1×10^{-3}	1.4×10^{-4}	6.2×10^{-4}
E	5.9×10^{-4}	6.4×10^{-4}	6.9×10^{-4}	8×10^{-4}	9.7×10^{-4}	1.7×10^{-4}	3.8×10^{-4}
	7.4×10^{-4}	8.1×10^{-4}	8.7×10^{-4}	1.1×10^{-3}	1.3×10^{-3}	2.6×10^{-4}	5.3×10^{-4}
F	4.8×10^{-4}	5.6×10^{-4}	6.1×10^{-4}	6.6×10^{-4}	8.6×10^{-4}	1.1×10^{-4}	3.7×10^{-4}
	5.9×10^{-4}	6.9×10^{-4}	7.6×10^{-4}	8.4×10^{-4}	1.2×10^{-3}	1.5×10^{-4}	6.2×10^{-4}
G	8×10^{-4}	9.6×10^{-4}	1×10^{-3}	1.1×10^{-3}	1.4×10^{-3}	1.1×10^{-4}	6.1×10^{-4}
	9.2×10^{-4}	1.1×10^{-3}	1.1×10^{-3}	1.2×10^{-3}	1.7×10^{-3}	1.4×10^{-4}	7.5×10^{-4}
H	9.3×10^{-4}	9.7×10^{-4}	1×10^{-3}	1.1×10^{-3}	1.3×10^{-3}	1.6×10^{-4}	3.9×10^{-4}
	1.1×10^{-3}	1.2×10^{-3}	1.2×10^{-3}	1.3×10^{-3}	1.6×10^{-3}	1.5×10^{-4}	5.1×10^{-4}
I	9.4×10^{-4}	1×10^{-3}	1.1×10^{-3}	1.1×10^{-3}	1.2×10^{-3}	8.8×10^{-5}	2.4×10^{-4}
	1.1×10^{-3}	1.2×10^{-3}	1.2×10^{-3}	1.3×10^{-3}	1.4×10^{-3}	8.8×10^{-5}	2.8×10^{-4}
J	8.9×10^{-4}	1.3×10^{-3}	1.4×10^{-3}	1.5×10^{-3}	1.8×10^{-3}	2.1×10^{-4}	9.2×10^{-4}
	1.1×10^{-3}	1.8×10^{-3}	1.9×10^{-3}	2.1×10^{-3}	2.4×10^{-3}	2.8×10^{-4}	1.3×10^{-3}
K	1.1×10^{-3}	1.4×10^{-3}	1.7×10^{-3}	1.8×10^{-3}	2.2×10^{-3}	4.2×10^{-4}	1.1×10^{-3}
	1.3×10^{-3}	1.8×10^{-3}	2×10^{-3}	2.2×10^{-3}	2.6×10^{-3}	4×10^{-4}	1.3×10^{-3}

Figure 6. Comparison of mean-based (*Ra*) and median-based (*Rm*) versions of *Average Roughness*. (**Top**): box-and-whiskers plots of samples per pavement type (along x-axis: A–K, colour coded) in data set II (multiple scans per sample, resampled to 10 mm average point distance) for mean-based (**left**) and for median-based (**right**) versions of the parameter (y-axis unit: m). (**Bottom**): Table of minimum (Min.), first quartile (1st Qu.), median, third quartile (3rd Qu.), maximum (Max.), interquartile range (Interqu. R.) and span of values per pavement (A–K) for the median-based (top) and mean-based (bottom) versions of *Average Roughness*.

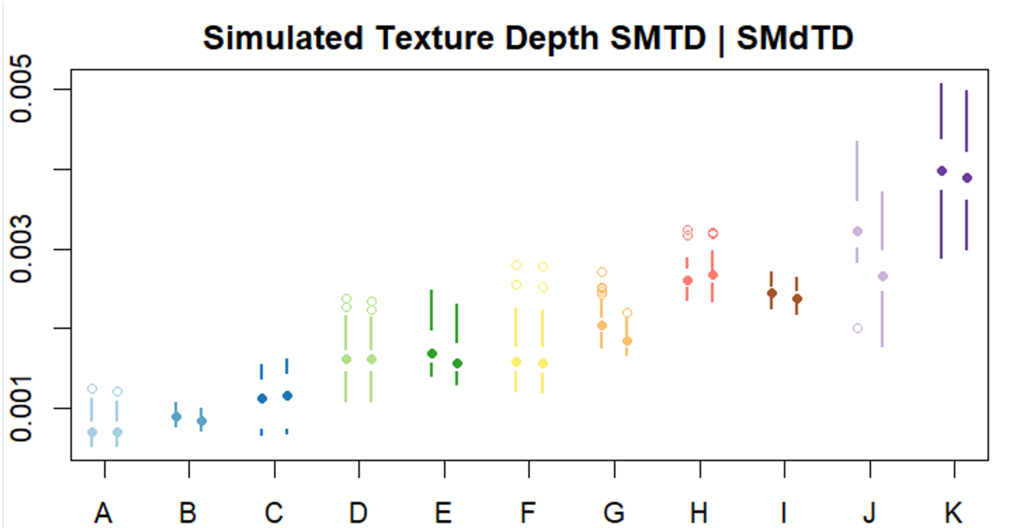

	Min.	1st Qu	Median	3rd Qu	Max.	Interqu. R.	Span
A	5.2×10^{-4}	6.4×10^{-4}	6.9×10^{-4}	8.4×10^{-4}	1.2×10^{-3}	2×10^{-4}	7×10^{-4}
	5.2×10^{-4}	6.4×10^{-4}	7×10^{-4}	8.4×10^{-4}	1.2×10^{-3}	2×10^{-4}	7.2×10^{-4}
B	7.2×10^{-4}	8.1×10^{-4}	8.4×10^{-4}	9×10^{-4}	1×10^{-3}	9×10^{-5}	2.9×10^{-4}
	7.7×10^{-4}	8.7×10^{-4}	8.9×10^{-4}	9.7×10^{-4}	1.1×10^{-3}	9.7×10^{-5}	3×10^{-4}
C	6.8×10^{-4}	7.5×10^{-4}	1.2×10^{-3}	1.4×10^{-3}	1.6×10^{-3}	7×10^{-4}	9.4×10^{-4}
	6.7×10^{-4}	7.4×10^{-4}	1.1×10^{-3}	1.4×10^{-3}	1.5×10^{-3}	6.4×10^{-4}	8.8×10^{-4}
D	1.1×10^{-3}	1.5×10^{-3}	1.6×10^{-3}	1.7×10^{-3}	2.3×10^{-3}	2.8×10^{-4}	1.3×10^{-3}
	1.1×10^{-3}	1.5×10^{-3}	1.6×10^{-3}	1.7×10^{-3}	2.4×10^{-3}	3×10^{-4}	1.3×10^{-3}
E	1.3×10^{-3}	1.5×10^{-3}	1.6×10^{-3}	1.8×10^{-3}	2.3×10^{-3}	3.7×10^{-4}	1×10^{-3}
	1.4×10^{-3}	1.6×10^{-3}	1.7×10^{-3}	2×10^{-3}	2.5×10^{-3}	4.2×10^{-4}	1.1×10^{-3}
F	1.2×10^{-3}	1.4×10^{-3}	1.6×10^{-3}	1.8×10^{-3}	2.8×10^{-3}	3.2×10^{-4}	1.6×10^{-3}
	1.2×10^{-3}	1.5×10^{-3}	1.6×10^{-3}	1.8×10^{-3}	2.8×10^{-3}	3.2×10^{-4}	1.6×10^{-3}
G	1.7×10^{-3}	1.8×10^{-3}	1.8×10^{-3}	1.9×10^{-3}	2.2×10^{-3}	1.6×10^{-4}	5.4×10^{-4}
	1.8×10^{-3}	2×10^{-3}	2×10^{-3}	2.1×10^{-3}	2.7×10^{-3}	1.8×10^{-4}	9.5×10^{-4}
H	2.3×10^{-3}	2.6×10^{-3}	2.7×10^{-3}	2.7×10^{-3}	3.2×10^{-3}	1.8×10^{-4}	8.7×10^{-4}
	2.4×10^{-3}	2.5×10^{-3}	2.6×10^{-3}	2.8×10^{-3}	3.2×10^{-3}	2.5×10^{-4}	8.8×10^{-4}
I	2.2×10^{-3}	2.3×10^{-3}	2.4×10^{-3}	2.5×10^{-3}	2.6×10^{-3}	1.7×10^{-4}	4.5×10^{-4}
	2.3×10^{-3}	2.4×10^{-3}	2.4×10^{-3}	2.5×10^{-3}	2.7×10^{-3}	1.6×10^{-4}	4.6×10^{-4}
J	1.8×10^{-3}	2.5×10^{-3}	2.7×10^{-3}	3×10^{-3}	3.7×10^{-3}	5.4×10^{-4}	1.9×10^{-3}
	2×10^{-3}	3×10^{-3}	3.2×10^{-3}	3.6×10^{-3}	4.4×10^{-3}	5.9×10^{-4}	2.3×10^{-3}
K	3×10^{-3}	3.6×10^{-3}	3.9×10^{-3}	4.2×10^{-3}	5×10^{-3}	6.1×10^{-4}	2×10^{-3}
	2.9×10^{-3}	3.7×10^{-3}	4×10^{-3}	4.4×10^{-3}	5.1×10^{-3}	6.6×10^{-4}	2.2×10^{-3}

Figure 7. Comparison of mean-based (*SMTD*) and median-based (*SMdTD*) versions of *Simulated Texture Depth*. (**Top**): box-and-whiskers plots of samples per pavement type (along x-axis: A–K, colour-coded) in data set II (multiple scans per sample, resampled to 10 mm average point distance) for mean-based (**left**) and for median-based (**right**) versions of the parameter (y-axis unit: m). (**Bottom**): Table of minimum (Min.), first quartile (1st Qu.), median, third quartile (3rd Qu.), maximum (Max.), interquartile range (Interqu. R.) and span of values per pavement (A–K) for the median-based (top) and mean-based (bottom) versions of *Simulated Texture Depth*.

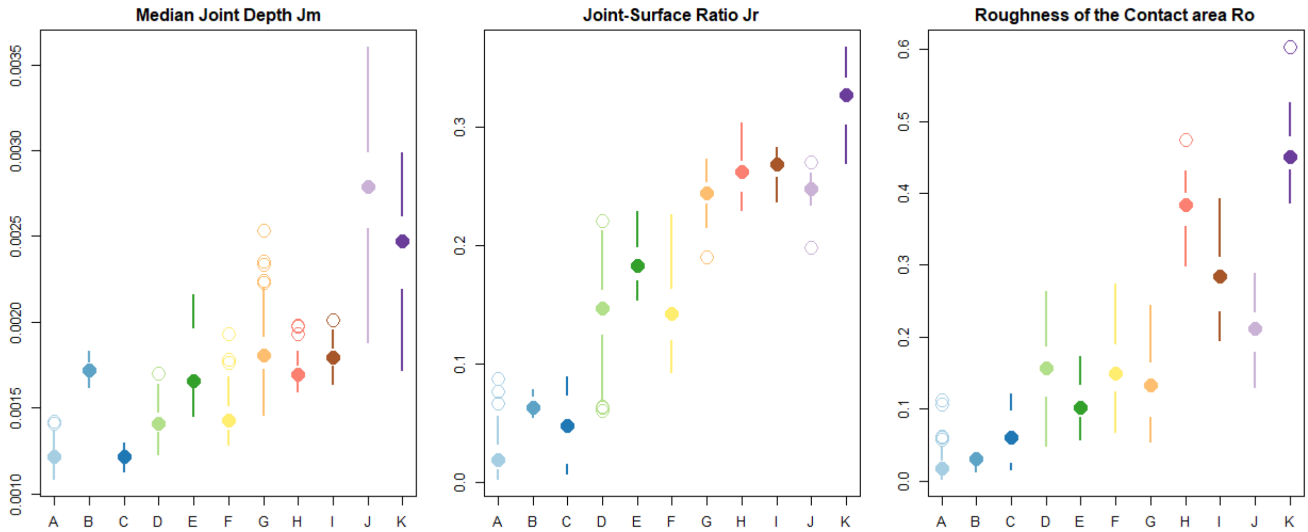

Figure 8. Box-and-whisker plots for parameter values of J_m (unit: m), J_r and R_o (unitless, theoretical range: 0–1) per pavement (along x-axis: A–K, colour-coded) in data set II (multi-scan, resampled to 10 mm average point distance).

In the following, two variables that potentially contribute to the observed within-type parameter variation are examined: the distance to the nearest laser scanning setup and the number of laser scanning setups covering the sample. The distance to the nearest laser scanning setup is expected to relate to the point density before resampling and to the prevalent intersection angle between the laser beam and the surface. It is expected that samples within short distances from the scanning station yield higher parameter values than those further away. The coverage by multiple laser scanning setups, on the other hand, may have diverse effects: improved point density, reduction of parameter values by the contribution from laser scanning setups with less favourable intersection geometries, but also levelling of effects caused by varying distances to the closest scanning station. We analyse the effect of pavement type, relative to potential effects of the distance to the nearest scanning station (*distance*) and the number of stations covering the sample (*coverage*), on parameter values for R_m, $SMdTD$, J_m, J_r, and R_o using a series of linear mixed-effects models. First, we briefly report on models fitted on the full data set II. Then, we present results from analysing a data set that was reduced to sampling units within 6 m from the nearest scanning station. The reason for this is that *distance* and *coverage* are strongly correlated in data set II (Figure 9): Samples with $coverage = 1$ are distributed along the entire range of *distance* (2–10 m) but occur most frequently beyond 6 m from the nearest station. Sampling units with $coverage = 2$, on the opposite, mostly have a $distance \leq 6$ m with a light skew of the distribution to the left. The same is true for sampling units with a $coverage > 2$, but for this group, the distribution is skewed to the right. However, most pavements do not include samples with a $coverage > 2$. Due to the correlation, any inference on either *distance* or *coverage* is difficult to assess. To eliminate the correlation, the data set was reduced to samples within 6 m from the closest scanning station.

All models initially contained a mean-centred variable *distance* and a treatment-coded (0,1) two-level factor for *coverage* (reference: $coverage = 1$, level 1: $coverage > 1$), as well as the interaction term of *distance* and *coverage*. The models also contained a random intercept for pavement (A–K). No random slopes were fitted because of the inhomogeneous distribution of samples along the full range of *distance* and the limited data density at $coverage = 1$ for some of the pavements (Figure 9). If the interaction between *distance* and *coverage* was not significant, we fitted a simpler model without it. The simplified model was compared to the full model via a likelihood ratio test. The final models were fitted using restricted maximum likelihood (REML) [50]. Because all models converged in their initial form, no transformation of the response variable (surface parameter values) was attempted (c.f. [51]). We report model coefficients, standard errors, and t-values for main effects and interactions; variance components and standard deviations for random effects; and bootstrapped confidence intervals for significant model coefficients, including random effects, at the 0.05 alpha level [52]. To explore the explanatory power of the model and its terms, we report marginal and conditional R^2 [53], together with intra-class correlation (ICC) for random effects [54] (Table 3). All analyses were carried out in R 4.5.2 [55] using package lme4 2.0-1 [56].

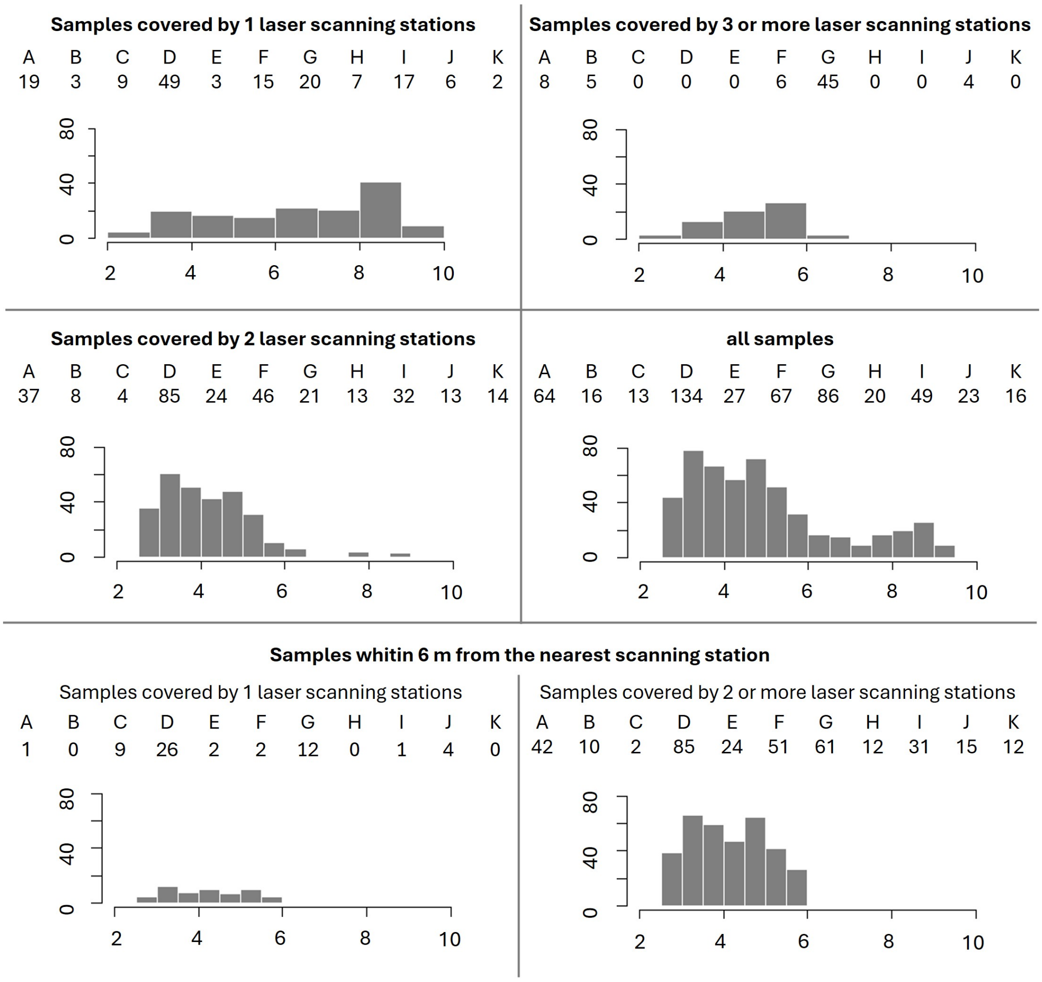

Figure 9. The distribution of surfaces samples across different pavements (A–K) and distance from the nearest laser scanning station (along the x-axis) for different coverage by scanning stations in data set II (**top**) and in reduced data set II with samples within 6 m from the nearest laser scanning station only (**bottom**).

Results from models fitted to of the full data set II (for details, see Supplementary Materials): All models yield significant random intercepts for pavement (i.e., the variance component of pavement type) and significant residual variance (unexplained variance). Also, the coefficient for *coverage* is significant in all models. Coverage by more than one scanning station results in smaller parameter values compared to coverage by one station. In the models for J_r and R_o, this is the only significant main effect. In the models for R_m and J_m, the interaction between *distance* and *coverage* is significantly negative as well. In the model for $SMdTD$, the coefficients of *coverage*, and *distance* and their interaction are significant. The interpretation of the coefficients is difficult. Due to the correlation of the variables *distance* and *coverage* in data set II, the effect of *coverage* cannot be disentangled from an influence of *distance*. However, in all models, the contribution of the main effects taken together (*coverage*, *distance*, and their interaction, if included) in explaining the variance of parameter values is minimal ($R^2 marginal \leq 0.01$) compared to the contribution of the random effects ($R^2 conditional > 0.91$). Over 90% of the variance in the data is attributed to pavement type according to the models ($ICC > 0.91$). Of course, this is not equal to a pairwise significant difference for all pavement types. But it demonstrates that pavement type is the most crucial factor in explaining the variance of the data using linear mixed-effects models.

Table 3. Results from linear mixed-effects model analyses.

R_m					
Fixed effects	Estimate	SE	t-value	$CI_{alpha=0.05}$	
intercept	8.54×10^{-4}	1.38×10^{-4}	6.196	$5.81 \times 10^{-4}, 1.13 \times 10^{-3}$	
coverage	-5.01×10^{-5}	1.52×10^{-5}	−3.286	$-8.00 \times 10^{-5}, -1.99 \times 10^{-5}$	
distance	-1.36×10^{-5}	5.58×10^{-6}	−2.437	$-2.47 \times 10^{-5}, -2.59 \times 10^{-6}$	
Random effects	Variance	Std. Dev.		$CI_{alpha=0.05}$	
intercept	2.07×10^{-7}	4.54×10^{-4}		$2.68 \times 10^{-4}, 6.66 \times 10^{-4}$	
residual	9.39×10^{-9}	9.69×10^{-5}		$9.01 \times 10^{-5}, 1.04 \times 10^{-4}$	
R^2 *marginal*	2.08×10^{-3}	R^2 *conditional*	9.57×10^{-1}	*ICC*	9.57×10^{-1}
SMdTD					
Fixed effects	Estimate	SE	t-value	$CI_{alpha=0.05}$	
intercept	2.01×10^{-3}	2.78×10^{-4}	7.237	$1.478 \times 10^{-3}, 2.56 \times 10^{-3}$	
coverage	-1.39×10^{-4}	2.98×10^{-5}	−4.658	$-1.97 \times 10^{-4}, -8.03 \times 10^{-5}$	
distance	-4.02×10^{-5}	1.09×10^{-5}	−3.684	$-6.17 \times 10^{-5}, -1.85 \times 10^{-5}$	
Random effects	Variance	Std. Dev.		$CI_{alpha=0.05}$	
intercept	$8.42e \times 10^{-7}$	9.18×10^{-4}		$5.47 \times 10^{-4}, 1.34 \times 10^{-3}$	
residual	3.60×10^{-8}	1.90×10^{-4}		$1.76 \times 10^{-4}, 2.037 \times 10^{-4}$	
R^2 *marginal*	4.09×10^{-3}	R^2 *conditional*	9.59×10^{-1}	*ICC*	9.59×10^{-1}
J_m					
Fixed effects	Estimate	SE	t-value	$CI_{alpha=0.05}$	
intercept	1.80×10^{-3}	1.43×10^{-4}	12.582	$1.51 \times 10^{-3}, 2.08 \times 10^{-3}$	
coverage	-7.07×10^{-5}	2.22×10^{-5}	−3.18	$-1.14 \times 10^{-4}, -2.78 \times 10^{-5}$	
distance	-1.46×10^{-5}	8.13×10^{-6}	−1.793		
Random effects	Variance	Std. Dev.		$CI_{alpha=0.05}$	
intercept	2.19×10^{-7}	4.68×10^{-4}		$2.79 \times 10^{-4}, 6.86 \times 10^{-4}$	
residual	2.00×10^{-8}	1.41×10^{-4}		$1.31 \times 10^{-4}, 1.51 \times 10^{-4}$	
R^2 *marginal*	3.21×10^{-3}	R^2 *conditional*	0.917	*ICC*	9.17×10^{-1}
J_r					
Fixed effects	Estimate	SE	t-value	$CI_{alpha=0.05}$	
intercept	1.90×10^{-1}	3.08×10^{-2}	6.169	$1.31 \times 10^{-1}, 2.50 \times 10^{-1}$	
coverage	-1.74×10^{-2}	3.28×10^{-3}	−5.307	$-2.39 \times 10^{-2}, -1.09 \times 10^{-2}$	
distance	-3.39×10^{-3}	1.20×10^{-3}	−2.828	$-5.73 \times 10^{-3}, -1.04 \times 10^{-3}$	
Random effects	Variance	Std. Dev.		$CI_{alpha=0.05}$	
intercept	1.03×10^{-2}	1.02×10^{-1}		$6.00 \times 10^{-2}, 1.49 \times 10^{-1}$	
residual	4.35×10^{-4}	2.09×10^{-2}		$1.94 \times 10^{-2}, 2.23 \times 10^{-2}$	
R^2 *marginal*	4.22×10^{-3}	R^2 *conditional*	0.960	*ICC*	9.60×10^{-1}
R_o					
Fixed effects	Estimate	SE	t-value	$CI_{alpha=0.05}$	
intercept	1.87×10^{-1}	4.32×10^{-2}	4.329	$1.04 \times 10^{-1}, 2.71 \times 10^{-1}$	
coverage	-7.26×10^{-3}	6.62×10^{-3}	−1.096		
distance	-3.92×10^{-3}	2.42×10^{-3}	−1.619		
Random effects	Variance	Std. Dev.		$CI_{alpha=0.05}$	
intercept	2.01×10^{-2}	1.42×10^{-1}		$8.46 \times 10^{-2}, 2.07 \times 10^{-1}$	
residual	1.77×10^{-3}	4.21×10^{-2}		$3.91 \times 10^{-2}, 4.51 \times 10^{-2}$	
R^2 *marginal*	8.50×10^{-4}	R^2 *conditional*	9.19×10^{-1}	*ICC*	9.19×10^{-1}

https://doi.org/10.3390/smartcities9090146

Results from models fitted to the reduced data set without correlation between *coverage* and *distance* (Table 3): All models yield significant random intercepts for pavement type as well as significant residual variance. In the models for R_m, $SMdTD$, and J_r, *coverage* and *distance* have a significant effect on parameter values. In the model for J_m, only *coverage* has a significant effect on parameter values, and in the model for R_o, none of the main effect coefficients are significant. Both $coverage > 1$ and *distance* reduce the values of roughness parameters. The coefficients for *coverage* are −3.9% (J_m), −5.8% (R_m), −6.9% ($SMdTD$) and −9.1% (J_r) of the respective estimated mean parameter value at mean distance and $coverage = 1$. The coefficients for *distance* are all below 2% of the respective estimated mean parameter value at mean *distance* and $coverage = 1$. Again, marginal $R^2 < 0.005$ and conditional $R^2 > 0.91$, together with the $ICC > 0.91$, imply that more than 91% of the variance in the data are explained by pavement type according to the models. The reduction of parameter values with increasing *distance* is in alignment with our expectations. With increasing *distance*, the intersection angle between the laser beam and the surface diminishes, and with it, the measurements of joints and depressions. However, the negative effect of *coverage* by multiple stations, independent of *distance*, is stronger. Again, the distance to the laser scanning setups is a likely explanation for this effect: *Distance* is measured to the nearest scanning station; therefore, every additional scanning setup that contributes to the sample is farther away and will add measurements with poorer intersection geometry.

4.3. Combining Information from Multiple Parameters

Individual parameters are not expected to adequately characterise pavements with respect to accessibility (c.f. [15]). We therefore combine the values of multiple parameters into a 1D aggregate measure that ranges from zero to five and ranks pavements in the order of descending roughness. To build the aggregate measure, we normalise the values of each parameter to the range between its theoretical minimum (zero for all parameters, corresponding to a perfectly smooth surface) and a theoretical maximum. The theoretical maximum is specific to each parameter: for R_o, it is the numerical maximum: 1. For J_r, the numerical maximum (1) cannot be reached, instead the maximum is set at 0.6. For R_m, $SMdTD$ and J_m, the theoretical maxima are informed by the guidelines on barrier-free infrastructure design: the guidelines limit the heights of steps that can be managed by wheelchair travellers to 20–30 mm. This threshold marks the contextual limit between the characterisation of a surface with respect to travelling comfort as opposed to obstacles. Therefore, the maximum for $SMdTD$ and J_m is set at 25 mm and the maximum for R_m is set at 12.5 mm, since R_m is expected to be approximately half the amount of $SMdTD$. With the same rationale behind it, a threshold of 25 mm was also applied in the filtering of outliers during parameter computation (c.f. Section 3.3). The ranking of pavement samples according to the proposed aggregate measure is shown in Figure 10. At the level of pavement-wise means, the aggregate measure mostly reflects the classification of surfaces according to Section 3.2. In addition, we apply classical metric dimensional scaling (MDS) [57] to explore the discriminative power of the combined parameters in a 2D space (Figure 11). MDS mostly separates samples from different pavements, while the distribution along the x-axis may reflect general roughness (as in R_m and $SMdTD$) and joint density J_r, the scattering along the y-axis may be explained by the roughness of the contact area (flat cobble stones: G and J vs. raw cobble stones: I vs. rounded boulders: H and K). The undesirable overlaps between samples of pavement C and D/F are due to adverse laser beam reflectance by the polished tiles of pavement C. The composite descriptor does not discriminate between pavements D and F. This could be because these pavements are indeed similar with respect to accessibility. It could also indicate limits in the

https://doi.org/10.3390/smartcities9090146

discriminative power of the proposed composite descriptor. When mapping the aggregate measure to geographic space, the resulting Figure 12 indicates a gradual transition between approximately seven groups of pavements, from smooth (1: A, C) to suitable (2: B) to ever rougher surfaces (3: D1; 4: D2, E, F; 5: G; 6: H, I, J; 7: K). However, some pavements display considerable variation and overlap with qualitatively distinct types (e.g., A–C with D and A–C with F).

In practice, it is unlikely that pavements will reach the theoretical maximum aggregate value of five. Pavement K is probably close to the practical maximum of pavement roughness. Also, unlike simple range normalization, the proposed scaling weights parameters according to their variance relative to their range. This is only justified if the theoretical maxima for parameters are reasonable. Estimating reasonable, practical upper thresholds for each parameter is a task for future studies in which an even larger diversity of pavements should be included. In addition, weighting is introduced by the redundancy of information in different parameters, namely R_m, $SMdTD$, and J_m. The proposed composite measure is an attempt to achieve a general assessment of pavement accessibility. For its application in personalised routing, it may be expedient to provide the possibility for a user-defined tuning of parameter weights, based on known pavements, to assess the accessibility of pavements at unknown locations.

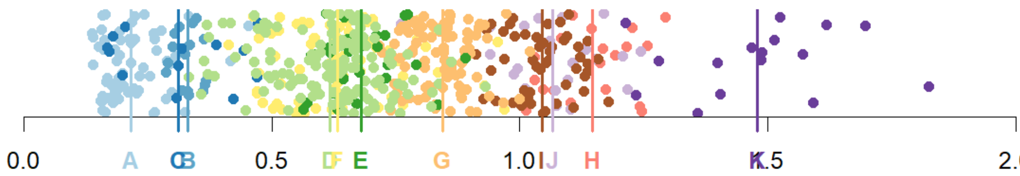

Figure 10. Additive measure from all parameters (theoretical value range: 0–5) calculated on data set II. Each parameter is scaled to the range of a theoretical minimum (0) and a theoretical maximum (R_m: 0.0125 m, $SMdTD$: 0.025 m, J_m: 0.0125 m, J_r: 0.6 and R_o: 1) and then added to the composite measure. The value for each sampling unit is plotted along the x-axis. The vertical scattering is random to improve readability. The circles are colour-coded according to pavement type (A–K). Letters indicate the mean values per pavement (A–K). Samples of different surface types are not necessarily expected to be separated without overlap, but overall ordering is expected to correspond to the ranking established in Section 3.2.

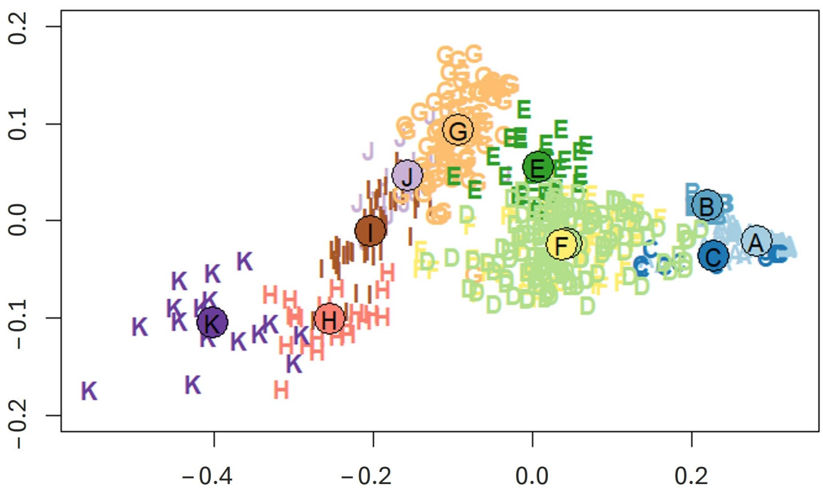

Figure 11. Result of metric multi-dimensional scaling on vectors of parameter values in data set II. Values for each parameter are scaled to the range of a theoretical minimum (0) and a theoretical maximum (R_m: 0.0125 m, $SMdTD$: 0.025 m, J_m: 0.0125 m, J_r: 0.6 and R_o: 1). Each sampling unit is plotted as a letter (A–K) indicating the pavement type. Circled letters are positioned at pavement means (A–K). Axes are unitless.

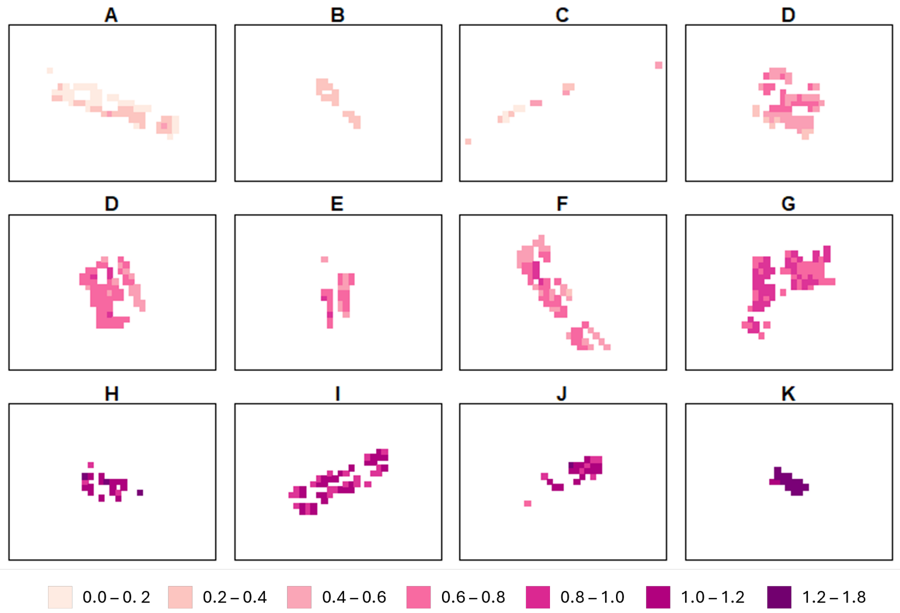

Figure 12. Additive measure from all surface roughness parameters (R_m, $SMdTD$, J_m, J_r, R_o) (theoretical value range: 0–5) for each pavement **A**–**K** mapped to geographic space (square = 1 m × 1 m). Map of surface type D is split across two plots, due to its non-continuous coverage. The bins of the colour scale are right closed.

5. Discussion

In the following, we discuss the potential and limits of our method and our results as well as the transferability to other data.

Since computation time increases with point density, the finding that values for R_m, $SMdTD$ and J_m remain stable ($CV \leq 5\%$) in data set I when the point cloud is resampled to an average point distance of 10 mm is encouraging. For J_r and R_o, the results on data set I indicate that resampling to 2 mm is a more cautious choice. However, these results only demonstrate the sensitivity of the analysed parameters to resampling. They do not imply that the original point cloud can be acquired at a lower point density. High-resolution scanning remains essential to preserve the complete surface information before resampling.

Although R_o was not stable under resampling in data set I, its variability in the real-world data set II remained low and was comparable to that of the other parameters. In fact, R_o is the only parameter for which a significant effect of *distance* to the scanning station is not observed, when the nearest scanning setup is within 6 m from the sample. Furthermore, this parameter seems to support the discrimination of different pavements via MDS (Figure 11). The results from data set II also indicate decreased within-pavement value ranges and increased pavement discrimination for the median-based versions of *Average Roughness* (R_m) and *Simulated Texture Depth* ($SMdTD$) compared to the mean-based parameters (R_a, $SMTD$). This suggests a stabilizing effect of the median, which was intended to help mitigate effects from varying distances to the scanning setups. Also, the ranking of pavement-wise median values by R_m and $SMdTD$ are plausible. It could be argued that J_r underestimates the joint-surface ratio in pavements with large, shallow joints, such as pavement D. However, the parameter values are within expectations considering its computation. Maybe, the definition of joint areas in the current parameter computation should be evaluated by wheelchair travellers. Depending on the result, additional criteria may be included to achieve an appropriate separation of joints and surfaces.

The application of the surface roughness parameters to a larger point cloud pooled from multiple laser scanning setups does not substantially change the ranking of pavements based on median parameter values. Moreover, pavement explains over 90% of the variance in parameter values according to our linear mixed-effects model analyses of data set II. However, parameter values show considerable within-pavement variation for most pavements. There are several potential sources of this variation. In the following, we discuss the different components of variance (Table 4), their potential influence on the surface roughness parameter values, and how they are considered in our analysis. First, some variance is introduced by the range noise of the laser scanner (0.4 mm at 10 m [26,42]). A probable effect of range noise would be an increase in R_m and $SMdTD$ values for smooth surfaces (e.g., A, B, and C). The contribution of range noise was not assessed in the current study and would require reference data acquired with a more accurate measurement technology. However, the median values of R_m and $SMdTD$ for smooth pavements (A, B, and C) are clearly below those of other pavements (D-K) in our data. Therefore, we conclude that range noise is not a factor inhibiting pavement accessibility characterisation based on the study data. Samples $\geq$ 8 m from the scanning stations might be more affected by range noise than others [26,42]. Therefore, it might be worthwhile restricting the data to points within 8 m of the scanning stations. A second source of variance is the sample location. This component includes variation introduced by the specific positioning of the sampling grid at the stage of point cloud sectioning and plane fitting. It also entails variance due to point cloud co-registration residuals (up to 8 mm in the present data). Neither of these effects was explicitly considered in the linear mixed-effects models, and both may contribute to the residual variance. The influence of sample location may partly be indicated by the results from the analysis of the 0.5 m $\times$ 0.5 m sub-cells. Potentially, a different neighbourhood shape could be applied to reduce undesirable parameter variation at the stage of point cloud sectioning and plane fitting. Distance from the laser scanning setup affects both point density and the laser beam-ground intersection. In data set II, variation in point density was reduced by resampling the original point cloud to an average point distance of 10 mm. The effect of resampling itself was examined in the analysis of data set I. Resampling the point cloud before computation of R_m, $SMdTD$ and J_m resulted in $CV \leq 5\%$, but higher values were observed for J_r and R_o. In contrast, variation in the laser beam-ground intersection remains related to scanning distance. Its contribution was therefore investigated using *distance* as a fixed effect in the linear mixed-effects models. The analysis revealed a significant effect of *distance* to the scanning stations on all surface roughness parameters except R_o. *Distance* therefore contributes to within-pavement variation in parameter values. However, its contribution is minor compared with that of pavement geometry according to the linear mixed-effects models. Thus, although scanning distance affects the parameter values, this effect does not prevent the characterisation of pavements regarding accessibility. Finally, we also expect true within-pavement variability, in particular for pavements with signs of wear (e.g., A, E and J), pavements with irregular layouts of stones (e.g., D, F, H and K), and pavements with raw surfaces (e.g., H, I and K). Overlapping parameter values between samples of different pavements, on the other hand, are not necessarily a cause for concern, as they may reflect similar surface properties. That said, our study also reveals potential sources of error in parameter values. Errors may arise from data quality issues, either due to highly reflective materials, such as pavement C, or due to artefacts from incomplete ground segmentation, as in pavement A. These effects were not explicitly considered in the linear mixed-effects models and may contribute to the residual variance. Thus, the residual variance may comprise both, true within-pavement variability and effects related to measurement, data quality, and processing, which cannot be separated based on the current analysis. Nevertheless, pavement type explains by far the largest part of the variance in parameter values according to the linear mixed-effects models.

It must be emphasised that our study targets surface characteristics that are at the limit of, or even beyond, the specified accuracy of the scanning technology used. Our results indicate, however, that differences between pavements can still be meaningfully characterised at the level of surface type averages. This suggests that the specified accuracy of individual measurements does not directly determine the ability to characterise surface types from aggregated point cloud properties. However, results for highly reflective materials need to be interpreted with care. Furthermore, we specifically developed the proposed method for use with TLS data and do not expect it to be transferable to data captured with other technologies without adaptation. Other measurement technologies may offer advantages over TLS for the assessment of surface roughness. However, off-the-shelf terrestrial laser scanners are widely used, whereas more specialised capturing technologies with similar or higher accuracy and resolution are less readily available. Our study demonstrates that high-density point clouds from TLS can nevertheless be used to assess the accessibility of various urban pavements with a high level of granularity compared with written guidelines. To characterise surfaces comprehensively, it is necessary to combine information on different properties and parameters. However, the proposed procedure for combining parameters to a multi-dimensional descriptor is preliminary. The current choice of theoretical maxima for range scaling is not ideal, since in practice, it is unlikely that urban pavements reach these thresholds. This reduces the discriminative power of the descriptor and introduces unintentional weighting of parameters. Also, the attained descriptor values do not provide an estimate of pavement accessibility with respect to the full scale of the descriptor (0–5). It must be emphasised that in the present data, only three pavements are clearly suited for wheelchair travel (A–C), and those pavements attain values $\leq$ 0.4 out of five. Therefore, although the study data covers a variety of pavements, additional data are needed to establish robust and transferable maxima for the scaling of parameters R_m, $SMdTD$, J_m, and J_r. Still, the present procedure allows for a detailed relative assessment of the pavements. It could help people extrapolate the suitability of pavements in unknown locations based on the parameter values of known pavements and thus assist in the choice of safe routes.

Table 4. Components of variance with an influence on surface roughness parameter values.

Components of Variance	Expected Direction of Influence on Surface Roughness Parameter Values	Treatment in the Analysis (Linear Mixed-Effects Models LMMs)
RTC360 range noise: 0.4 mm at 10 m	May increase parameter values, particularly for smooth surfaces	Not assessed; requires an external reference acquired with a more accurate measurement technology
Point cloud co-registration residuals (mean: 4 mm, max.: 8 mm)	May introduce random variation in parameter values; no systematic direction expected	Not explicitly considered; may contribute to residual variance in the LMMs
Point cloud sectioning	May introduce random variation in parameter values depending on the positioning of the sampling grid; no systematic direction expected	Not explicitly considered; may contribute to residual variance in the LMMs
Distance from the scanning station	Influences parameter values through several distance-dependent effects, including point density and laser beam-ground intersection	Considered as fixed effect *distance* (& *coverage*) in the LMMs
Point density 6 mm at 10 m	Depending on surface geometry, higher point density may increase parameter values; point density decreases with distance from the scanning station	Considered through resampling to an average point distance of 10 mm
Leaser beam-ground intersection	Increasing footprint size may decrease parameter values by smoothing small-scale surface variations; effect depends on surface geometry and scanning geometry	Indirectly considered through the fixed effect *distance* (& *coverage*)
Surface geometry	Greater true surface roughness results in higher parameter values	Considered through pavement random intercepts; true within-pavement variability also contributes to residual variance in the LMMs
Noise from non-ground points	May increase parameter values	Not explicitly considered; may contribute to residual variance in the LMMs
Reflectivity of surface material	High reflectivity may increase parameter values due to measurement artefacts	Not explicitly considered; may contribute to residual variance in the LMMs

6. Conclusions

With our work, we aimed at the identification of surface roughness parameters that are suited for the analysis of pavements in large-scale, high-density point clouds of urban areas recorded with off-the-shelf TLS technologies. The advantage of the proposed approach is its independence from a classification according to known pavement types as well as the consideration of gradual pavement degradation, gutters, manhole coverings, and other irregular structures affecting surface smoothness.

We explored the sensitivity of different surface roughness parameters with respect to point cloud resampling and varying distance to the laser scanning setup. Our results indicate that, at a specific distance from the scanning station, parameters R_a, R_m, $SMTD$, $SMdTD$, and J_m are stable with respect to absolute values and ranking of pavements when the point cloud is resampled to an average point distance of 10 mm. For parameters J_r and R_o, resampling to a 2 mm average point distance is a more cautious choice. The unstable behaviour of R_o related to point cloud resampling deserves further investigation. Using median-based *Average Roughness* (R_m) and *Simulated Texture Depth* ($SMdTD$) does not make parameters more stable with respect to resampling. It leads, however, to a reduction of the within-pavement value ranges. This reduction is more pronounced for R_m relative to R_a than it is for $SMdTD$ relative to $SMTD$. For all parameters, the ranking of pavements based on the median of all samples in data set II is meaningful overall. Parameter J_r may be refined in consultation with wheelchair users regarding its expressiveness with respect to the targeted accessibility criteria. Distance from the scanning station contributes significantly to within-pavement parameter value variation. Within-pavement parameter value variation may partly be driven by the contribution of scanning stations further than 6 m from the respective ground sample. Restricting the data to points within 8 m from the scanning station (instead of 10 m) may mitigate some of the effect. Despite the within-type variance, pavement type explains by and large most of the variance in the data according to the linear mixed-effects models. Also, reliable parameter computation relies on a clean point cloud of the pavement surface. Highly reflective surfaces that scatter the laser signal or artefacts from point cloud segmentation can lead to error. Still, results from metric MDS applied to a composite surface descriptor indicate that the combination of several roughness parameters is a promising way to characterise surface quality with respect to accessibility. We will integrate the findings in our work on large-scale micro-accessibility analysis. The proposed approach demonstrates how smart cities could benefit from the availability of accurate and high-resolution point cloud data for the digital assessment of accessibility at the micro-level.

Supplementary Materials: The following supporting information can be downloaded at https://www.mdpi.com/article/10.3390/smartcities9090146/s1, Table S1: Results of the linear mixed-effects model fitting on the full data set II.

Author Contributions: Conceptualization, D.H. and S.B.; methodology, D.H., M.A., and S.B.; investigation, D.H. and M.A.; data curation, M.A.; writing—original draft preparation, D.H., M.A., D.E.G., and S.B.; writing—review and editing, D.H., M.A., D.E.G., and S.B.; visualization, D.H.; supervision, D.E.G. and S.B.; project administration, D.E.G. and S.B.; funding acquisition, D.E.G. and S.B. All authors have read and agreed to the published version of the manuscript.

Funding: This work was completed as part of an industry funded research collaboration between the FHNW Institute Geomatics and Hexagon | Leica Geosystems.

Data Availability Statement: The data and code presented in this study are not publicly available due to the confidentiality requirements for unfinished re-search projects. Further inquiries can be directed to the corresponding author.

Acknowledgments: We thank the canton of Basel-Stadt for their ongoing interest in this area of research. Some preliminary work on the point cloud data were completed during a Bachelor Thesis Project at the FHNW Institute Geomatics including advice by the Pro Infirmis Fachstelle Hindernisfreies Bauen, Basel. We thank the reviewers for their valuable advice which helped to greatly improve our paper.

Conflicts of Interest: The authors declare no conflicts of interest. While the research reported here was completed as part of an industry funded research collaboration, the contents have not been influenced by industry interests but follow research questions deemed interesting in terms of data analysis and contributing to more accessible cities. Hexagon technologies were used for data collection and processing, but similar data can be collected with other technologies as indicated in Section 3.1.

References

1. Baobeid, A.; Koç, M.; Al-Ghamdi, S. Walkability and its relationships with health, sustainability, and liveability: Elements of physical environment and evaluation frameworks. *Front. Built Environ.* **2021**, *7*, 721218. [CrossRef]
2. Forsyth, A. What is a walkable place? The walkability debate in urban design. *Urban Des. Int.* **2015**, *20*, 274–292. [CrossRef]
3. Kockelman, K.; Zhao, Y.; Heard, L.; Taylor, D.; Taylor, B. The nature of ADA's sidewalk cross-slopes requirements: A review of the literature. *Transp. Res. Rec.* **2000**, *1705*, 53–60. [CrossRef]
4. Sze, N.N.; Christensen, K.M. Access to urban transportation system for individuals with disabilities. *IATSS Res.* **2017**, *41*, 66–73. [CrossRef]
5. Kapsalis, E.; Jaeger, N.; Hale, J. Disabled-by-design: Effects of inaccessible urban public spaces on users of mobility assistive devices—A systematic review. *Disabil. Rehabil. Assist. Technol.* **2024**, *19*, 604–622. [CrossRef] [PubMed]
6. Schmidt, E.; Manser, J. Strassen-Wege-Plätze. In *Richtlinien Behindertengerechte Fusswegnetze. 2. überarbeitete Auflage*; Schweizerische Fachstelle für behindertengerechtes Bauen, Ed.; Druckerei Albisrieden: Zürich, Switzerland, 2024.
7. *SN 640 075*; Fussgängerverkehr. Hindernisfreier Verkehrsraum, Erläuterungen, Anforderungen, Abmessungen. Normativer Anhang. Schweizerischer Verband der Strassen- und Verkehrsfachleute (VSS): Zürich, Switzerland, 2014.
8. Meyers, A.R.; Anderson, J.J.; Miller, D.R.; Shipp, K.; Hoenig, H. Barriers, facilitators, and access for wheelchair users: Sbstantive and methodologic lessons from a pilot study of environmental effects. *Soc. Sci. Med.* **2002**, *55*, 1435–1446. [CrossRef] [PubMed]
9. Matthews, H.; Beale, L.; Picton, P.; Briggs, D. Modelling Access with GIS in Urban Systems (MAGUS): Capturing the experiences of wheelchair users. *Area* **2003**, *35*, 34–45. [CrossRef]
10. Bromley, R.D.; Matthews, D.L.; Thomas, C.J. City centre accessibility for wheelchair users: The consumer perspective and the planning implications. *Cities* **2007**, *24*, 229–241. [CrossRef]
11. Saha, M.; Saugstad, M.; Maddali, H.T.; Zeng, A.; Holland, R.; Bower, S.; Dash, A.; Chen, S.; Li, A.; Hara, K.; et al. Project sidewalk: A web-based crowdsourcing tool for collecting sidewalk accessibility data at scale. In Proceedings of the 2019 CHI Conference on Human Factors in Computing Systems, Scotland, UK, 4–9 May 2019; pp. 1–14.
12. Laberee, K.; Nelson, T.; Boss, D.; Ferster, C.; Hosford, K.; Fuller, D.; Cloutier, M.S.; Winters, M. WalkRollMap.org: Crowdsourcing barriers to mobility. *Front. Rehabil. Sci.* **2023**, *4*, 1023582. [CrossRef] [PubMed]
13. Levesque, W.; Bégin-Drolet, A.; Lépine, J. Effects of pavement characteristics on rolling resistance of heavy vehicles: A literature review. *Transp. Res. Rec.* **2023**, *2677*, 296–309. [CrossRef]
14. Ejsmont, J.; Owczarzak, W. Engineering method of tire rolling resistance evaluation. *Measurement* **2019**, *145*, 144–149. [CrossRef]
15. Ejsmont, J.; Ronowski, G.; Świeczko-Żurek, B.; Sommer, S. Road texture influence on tyre rolling resistance. *Road Mater. Pavement Des.* **2017**, *18*, 181–198. [CrossRef]
16. Schlatter, F.; Schindler, J.; Bühlmann, E. Rollwiderstand auf Lärmarmen Belägen in der Schweiz. Einflussgrössen und CO_2-Emissionsbetrachung. Technical Report, G+P Ingenieure, Bundesamt für Umwelt Bafu. 2021. Available online: https://www.bafu.admin.ch/dam/de/sd-web/jUagOFi1NM2L/Rollwiderstand%20auf%20l%C3%A4rmarmen%20Bel%C3%A4gen%20in%20der%20Schweiz.pdf (accessed on 22 July 2026).
17. Mokrenko, V.; Yu, H.; Raychoudhury, V.; Edinger, J.; Smith, R.O.; Gani, M.O. A transfer learning approach to surface detection for accessible routing for wheelchair users. In *Proceedings of the 2021 IEEE 45th Annual Computers, Software, and Applications Conference (COMPSAC)*; IEEE: Madrid, Spain, 2021; pp. 794–803.
18. Silva, H.; Fonseca, F.; Rodrigues, A.; Palha, C. Engineering-based evaluation of sidewalk pavement materials: Implications for pedestrian safety and comfort. *Int. J. Pavement Res. Technol.* **2025**, *19*, 2454–2475. [CrossRef]
19. Waechter, M.; Riess, F.; Zacharias, N. A multibody model for the simulation of bicycle suspension systems. *Veh. Syst. Dyn.* **2002**, *37*, 3–28. [CrossRef]
20. Senthilvelan, J.; Izuo, H.; Endo, T.; Ueno, A. Relationship between surface material indices and skid resistance of concrete pavement. *Constr. Build. Mater.* **2024**, *449*, 138435. [CrossRef]

21. Edmondson, V.; Woodward, J.; Lim, M.; Kane, M.; Martin, J.; Shyha, I. Improved non-contact 3D field and processing techniques to achieve macrotexture characterisation of pavements. *Constr. Build. Mater.* **2019**, *227*, 116693. [CrossRef]
22. Li, L.; Wang, K.C.; Li, Q.J. Geometric texture indicators for safety on AC pavements with 1 mm 3D laser texture data. *Int. J. Pavement Res. Technol.* **2016**, *9*, 49–62. [CrossRef]
23. Tonietto, L.; Gonzaga, L., Jr.; Veronez, M.R.; Kazmierczak, C.d.S.; Arnold, D.C.M.; Costa, C.A.d. New method for evaluating surface roughness parameters acquired by laser scanning. *Sci. Rep.* **2019**, *9*, 15038. [CrossRef] [PubMed]
24. Edmondson, V.; Ardill, O.; Martin, J.; Lim, M.; Kane, M.; Woodward, J. Quantifying long-term rates of texture change on road networks. *Int. J. Pavement Eng.* **2022**, *23*, 1957–1969. [CrossRef]
25. Jiang, S.; Wang, H.; Fan, W.; Chi, M.; Zhang, X.; Ma, J. A Non-Contact method for detecting and evaluating the Non-Motor use of sidewalks based on Three-Dimensional pavement morphology analysis. *Sensors* **2025**, *25*, 1721. [CrossRef] [PubMed]
26. Geosystems, H.L. Leica Cyclone Register 360 Plus—3D Laser Scanning Point Cloud Registration Software. Fast Agile Precise. Data Sheet 872750en—04.22. Hexagon. 872750en—04.22 ed. 2022. Available online: https://leica-geosystems.com/products/laser-scanners/scanners/leica-rtc360 (accessed on 19 November 2024).
27. Gani, M.O.; Raychoudhury, V.; Edinger, J.; Mokrenko, V.; Cao, Z.; Zhang, C. Smart surface classification for accessible routing through built environment: A crowd-sourced approach. In Proceedings of the 6th ACM International Conference on Systems for Energy-Efficient Buildings, Cities, and Transportation, New York, NY, USA, 13–14 November 2019; pp. 11–20.
28. Edinger, J.; Hofmann, A.; Wachner, A.; Becker, C.; Raychoudhury, V.; Krupitzer, C. Wheelshare: Crowd-sensed surface classification for accessible routing. In Proceedings of the 2019 IEEE International Conference on Pervasive Computing and Communications Workshops (PerCom Workshops), Kyoto, Japan, 11–15 March 2019; pp. 584–589.
29. Mascetti, S.; Civitarese, G.; El Malak, O.; Bettini, C. SmartWheels: Detecting urban features for wheelchair users' navigation. *Pervasive Mob. Comput.* **2020**, *62*, 101115. [CrossRef]
30. Banerjee, R.; Islam, M.F.; Saha, S.; Raychoudhury, V.; Gani, M.O. Surface recognition from wheelchair-induced noisy vibration data: A tale of many cities. In Proceedings of the 2022 18th International Conference on Mobility, Sensing and Networking (MSN), Guangzhou, China, 14–16 December 2022; pp. 619–626.
31. Tong, X.; Simoni, M.D.; Arfvidsson, K.M.; Mårtensson, J. Leveraging sidewalk robots for walkability-related analyses. *Comput. Environ. Urban Syst.* **2026**, *124*, 102381. [CrossRef]
32. Weld, G.; Jang, E.; Li, A.; Zeng, A.; Heimerl, K.; Froehlich, J.E. Deep learning for automatically detecting sidewalk accessibility problems using streetscape imagery. In Proceedings of the 21st International ACM SIGACCESS Conference on Computers and Accessibility, Pittsburgh, PA, USA, 28–30 October 2019; pp. 196–209.
33. Hosseini, M.; Miranda, F.; Lin, J.; Silva, C.T. CitySurfaces: City-scale semantic segmentation of sidewalk materials. *Sustain. Cities Soc.* **2022**, *79*, 103630. [CrossRef]
34. Treccani, D.; Díaz-Vilariño, L.; Adami, A. Sidewalk detection and pavement characterisation in historic urban environments from point clouds: Preliminary results. *Int. Arch. Photogramm. Remote Sens. Spat. Inf. Sci.* **2021**, *43*, 243–249. [CrossRef]
35. Santos, P.M.; Júlio, E.N. A state-of-the-art review on roughness quantification methods for concrete surfaces. *Constr. Build. Mater.* **2013**, *38*, 912–923. [CrossRef]
36. Wang, C.; He, S.; Fang, X.; Han, J.; Liu, Z.; Ning, X.; Li, W.; Tiwari, P. Point Clouds Meets Physics: Dynamic Acoustic Field Fitting Network for Point Cloud Understanding. In Proceedings of the 2025 IEEE/CVF Conference on Computer Vision and Pattern Recognition (CVPR), Nashville, TN, USA, 11–15 June 2025; p. 22182. [CrossRef]
37. *ASTM E2157-15(2024)*; Standard Test Method for Measuring Pavement Macrotexture Properties Using the Circular Track Meter. Technical Report ASTM E2157-15(2024); ASTM International: West Conshohocken, PA, USA, 2024.
38. *ASTM E965-15(2019)*; Standard Test Method for Measuring Pavement Macrotexture Depth Using a Volumetric Technique. Technical Report ASTM E965-15(2019); ASTM International: West Conshohocken, PA, USA, 2024.
39. Bitelli, G.; Simone, A.; Girardi, F.; Lantieri, C. Laser scanning on road pavements: A new approach for characterizing surface texture. *Sensors* **2012**, *12*, 9110–9128. [CrossRef] [PubMed]
40. *ISO 25178-2:2021*; Geometrical Product Specifications (GPS)—Surface Texture: Areal. Part 2: Terms, Definitions and Surface Texture Parameters. Technical Report ISO 25178-2:2021; International Organization for Standardization: Vernier, Switzerland, 2021.
41. Berger, M.; Tagliasacchi, A.; Seversky, L.; Alliez, P.; Levine, J.; Sharf, A.; Silva, C. State of the art in surface reconstruction from point clouds. In Proceedings of the Eurographics 2014—State of the Art Reports, Strasbourg, France, 7–11 April 2014; pp. 161–185.
42. Bauer, P.; Woschitz, H. Laboratory Investigations of the Leica RTC360 Laser Scanner—Distance Measuring Performance. *Sensors* **2024**, *24*, 3742. [CrossRef] [PubMed]
43. Biasion, A.; Moerwald, T.; Walser, B.; Walsh, G. A new approach to the Terrestrial Laser Scanner workflow: The RTC360 solution. In Proceedings of the FIG Working Week, Hanoi, Vietnam, 22–26 April 2019.
44. Geosystems, H.L. Leica Cyclone Register 360 Plus—3D Laser Scanning Point Cloud Registration Software. Hexagon. 2022. Available online: https://leica-geosystems.com/products/laser-scanners/software/leica-cyclone/leica-cyclone-register-360 (accessed on 19 November 2024).

45. *SIA 500*; Hindernisfreie Bauten. Technical Report SIA 500; SIA: Zürich, Switzerland, 2009.
46. Pestalozzi, C.; Conrad, V.; Schimdt, E.; Manser, J.A.; Rüdisuli, B. *Hindernisfreier Verkehrsraum—Anforderungen aus Sicht von Menschen mit Behinderung*; Technical Report VSS 2008/201; International Organization for Standardization: Zürich, Switzerland, 2021. Available online: https://hindernisfreie-architektur.ch/wp-content/uploads/2025/10/HindernisfreierVerkehrsraum1308.pdf (accessed on 31 August 2026).
47. Cadotsch, L.; Karabasoglu, E. Hochaufgelöste 3D-Modelle für die Analyse der Accessibility. Bachelor's Thesis, FHNW, Muttenz, Switzerland, 2023.
48. Geosystems, H.L. Leica Cyclone 3DR. Hexagon. 2023. Available online: https://leica-geosystems.com/products/laser-scanners/software/leica-cyclone/leica-cyclone-3dr (accessed on 19 November 2024).
49. Harris, C.R.; Millman, K.J.; Van Der Walt, S.J.; Gommers, R.; Virtanen, P.; Cournapeau, D.; Wieser, E.; Taylor, J.; Berg, S.; Smith, N.J.; et al. Array programming with NumPy. *Nature* **2020**, *585*, 357–362. [CrossRef] [PubMed]
50. Meteyard, L.; Davies, R.A. Best practice guidance for linear mixed-effects models in psychological science. *J. Mem. Lang.* **2020**, *112*, 104092. [CrossRef]
51. Brauer, M.; Curtin, J.J. Linear mixed-effects models and the analysis of nonindependent data: A unified framework to analyze categorical and continuous independent variables that vary within-subjects and/or within-items. *Psychol. Methods* **2018**, *23*, 389. [CrossRef] [PubMed]
52. Bates, D.; Mächler, M.; Bolker, B.; Walker, S. Fitting linear mixed-effects models using lme4. *J. Stat. Softw.* **2015**, *67*, 1–48.
53. Nakagawa, S.; Schielzeth, H. A general and simple method for obtaining R^2 from generalized linear mixed-effects models. *Methods Ecol. Evol.* **2013**, *4*, 133–142. [CrossRef]
54. Nakagawa, S.; Schielzeth, H. Repeatability for Gaussian and non-Gaussian data: A practical guide for biologists. *Biol. Rev.* **2010**, *85*, 935–956. [CrossRef]
55. R Core Team. *R: A Language and Environment for Statistical Computing*; R Foundation for Statistical Computing: Vienna, Austria, 2025.
56. Bates, D.; Mächler, M.; Bolker, B.; Walker, S. lme4: Linear Mixed-Effects Models Using "Eigen" and S4. 2026. Available online: https://CRAN.R-project.org/package=lme4 (accessed on 10 July 2026).
57. Team, R.C. Classical (Metric) Multidimensional Scaling. 2026. Available online: https://stat.ethz.ch/R-manual/R-devel/library/stats/html/cmdscale.html (accessed on 22 July 2026).